Cape Peninsula University of Technology

Energy efficiency of solar heat concentrators using glass coated Al doped ZnO transparent conducting oxide as selective absorber

---

By
Abdalla Suliman Sasi

Thesis submitted in fulfilment of the requirements for the degree

Master of Technology: Mechanical Engineering

in the Faculty of Engineering at the

Cape Peninsula University of Technology

Supervisor: Dr.O. Nemraoui

Bellville campus

September 2017

DECLARATION

I, Abdalla Suliman Sasi declare that the contents of this thesis represent my own unaided work, and that the thesis has not previously been submitted for academic examination towards any qualification. Furthermore, it represents my own opinions and not necessarily those of the Cape Peninsula University of Technology.

Signed **Date**

ABSTRACT

Transparent conductive oxides (TCOs), which are widely used in transparent electronics, possess a spectral selectivity that is suitable for a solar material absorber. TCO materials have a plasma wavelength in the infrared region. Consequently electromagnetic waves shorter than a plasma wavelength are transmitted through the material, while longer electromagnetic waves are reflected on the surface. In contrast to the opaque solar selective absorbers, the plasma wavelength in TCO materials can be easily tuned by controlling the heavy doping process to match the peak shift of thermal radiation at higher temperatures. Furthermore, the use of TCO in conjunction with a solar absorber relaxes the spectral selectivity of the latter and thus widens the selection of the solar absorber; subsequently the only requirement is a thermally stable black body.

Aluminum doped Zinc Oxide (AZO) is a class of TCO materials which is cost effective to manufacture due to abundance ZnO, and Aluminum raw materials. This thesis is based on the synthesis of Al doped ZnO thin films nanostructure using radio frequency RF magnetron sputtering process. The influence of the deposition parameters, including argon working pressure and substrate temperature, on the structural and optical properties of the AZO thin films is investigated by means of X-ray diffraction (XRD) and optical spectroscopy (UV-VIS-NIR). The optical constants of AZO films are extracted from transmittance and reflectance spectra using a combination of Drude and Lorentz dielectric function model. A computer simulation is developed to calculate the radiative properties of Al doped ZnO thin films nanostructure. The thermal emittance and solar absorptance is predicted indirectly from optical reflectance and transmittance of AZO films by invoking Kirchhoff's law. A Special attention has been paid to the parameters that influence the spectral properties of the AZO films including carrier's mobility, Al doping concentration and film thickness. Carrier's mobility turned out to have the most significant influence on the spectrally selective performance of AZO films

.

ACKNOWLEDGEMENTS

I wish to thank and express my gratitude to Dr.O. Nemraoui for his supervision of this thesis. I wish to thank him for all his advice, counselling, support, guidance and constructive criticism which helped to accomplish this work.

I also wish to thank the staff of the Mechanical Engineering Workshop for their assistance.

Special thanks to my colleagues (postgraduate students) whom I have had the pleasure of knowing, have had discussions with and shared knowledge.

Great thanks for all my family members

DEDICATION

This thesis is dedicated to my loved ones, with a special feeling of gratitude to my loving mother and sisters, who have been a constant source of support and encouragement during the challenges of graduate school and life. To my wife who has always loved me unconditionally and whom I am truly thankful. Finally, to my wonderful daughters and sons for being there for me throughout the entire master's program. You have all been my best cheerleaders.

Thank you!**!**

TABLE OF CONTENTS

LIST OF FIGURES

LIST OF TABLES

LIST OF SYMBOLS, CONSTANTS AND ABBREVATIONS

A_a	Area of solar collector
TCO	Transparent Conducting Oxide
FTO	Fluorine Tin Oxide
A_γ	Area of energy absorber
C	Concentration ration for solar collectors
c	Speed of propagation of a wave in a medium
c_0	Speed of light under vacuum
E	Emissive power
e	Electronic charge
G	Irradiation
h	Planck's constant
I	Total radiation intensity
I_{sc}	Solar constant
k	Boltzmann's constant
m_e^*	Effective mass of the charge carriers
n	Index of refraction of a medium
N	Concentration of conduction band electrons
Q_e	Rate of emission of radiant energy
R	Reflectivity of TCO layer
T	Absolute temperature
α	Absorptivity
γ	Frequency of collision given
δ	Skin depth
ε	Emissivity
ϵ	Relative permittivity
ϵ’	Imaginary part of Drude’s theory
ϵ”	Real part of Drude’s theory
λ	Wavelength
λ_{pl}	Plasma resonance wavelength
μ	Electron mobility
v	Frequency of a wave
ρ	Reflectivity
σ	Stefan Boltzmann constant

τ	Transmitivity
τ_e	Relaxation time
ω	Optical frequency
ω_p	Plasma resonance frequency
λ	Wavelength
h	Plank's constant, 6.626 *10^{-34} Js
K_B	Boltzman's constant, 1.382*10-23 J/k
c	Speed of light
CSP	Concentrating solar power
t	Time
$\dot{P}$	Power
R	Reflectance
A	Absorbance
T	Transmittance
ε	Emittance
α	Absorptance

Subscripts

e = quantity is emitted

i = quantity is incident

b = property related to a blackbody

λ = indicate spectral nature of quantity of interest

θ = indicate direction nature of quantity of interest

CHAPTER ONE

INTRODUTION

1.1 Background

Increasing awareness of the depletion of fossil energy resources, as well as damage to the atmosphere by the emission of carbon dioxide when these resources are used as a source of energy, is increasingly resulting in the use of renewable energy sources instead. Solar energy is one such renewable energy source, and in particular concentrating solar power (CSP) systems, which are widely used.

Such CSP systems convert solar energy into electrical energy and can supply a significant amount of electrical energy without pollution of the atmosphere.

The feasibility of CSP technology has already been proven. The basic principle of this technology is that solar radiation is converted to thermal energy by means of a selective absorber. The key properties of a selective absorber are a high absorptance in the visible light range and a low emittance in the mid-far infrared range.

To improve the conversion efficiency in CSP plants and to meet the low cost target, an increase in the operating temperature of the carrier fluid is desirable. Current selective absorber coatings however, lack the desired thermal stability and performance to operate at higher temperatures; this lack is caused by oxidation, high humidity, corrosion, and particularly poor interlayer adhesion which leads usually to spectral selectivity degradation.

The quest for-long term thermal stability has driven many researchers to develop new high-temperature selective absorbers based on nitride, carbide and platinum-doped dielectric thin-film coatings, regardless of the cost. Nevertheless, at high temperatures the absorber must exhibit rigorous spectral selectivity since the peak of the thermal radiation spectrum shifts toward shorter wavelengths; that is toward near infrared radiation. This selectivity requirement needs a laborious and expensive fabrication process.

Material extensively applied in transparent electronics, are transparent conductive oxides (TCOs); possess the spectral selectivity suitable for solar absorber material. TCO materials have a plasma wavelength in the infrared region. Consequently, electromagnetic waves shorter than a plasma wavelength are transmitted through the material, while longer electromagnetic waves are reflected on the surface. In contrast to traditional solar selective absorbers, the plasma wavelength in TCO materials can be easily tuned by controlling the heavy doping process to match the peak shift of thermal radiation at higher temperatures.

Furthermore, the use of TCO in conjunction with a solar absorber relaxes the spectral selectivity of the latter and thus widens the selection of the solar absorber, since the only requirement is a thermally stable black body.

There is a dearth of information in the literature on the use of TCO coatings for solar selective absorbers at high temperatures. The results of a recent study relating to CSP systems, indicated that refractory materials coated with TCO materials displayed good spectral selectivity; typically, they remained thermally stable under vacuum conditions at 600°C for three hours, with a high absorptance of 0.71, and a low emittance 0.11 (Shimizu, Suzuki, Iguchi, & Yugami, 2014). However, as noted by (Mattox, 2010), it well known in the semiconductor industries thin-film tandems are prone to interfacial diffusion at high temperature which can hinder their thermal stability in the long term.

The aim of this project will be to decouple TCO material from the absorber to avoid high-temperature interdiffusion. This will be done by using TCO coated glass as low emittance heat trap and studying the photo-thermal efficiency of the system.

1.2 Keywords

Transparent conductive oxide, solar absorber, collectors, emissivity, thermal efficiency.

1.3 Energy sources

Energy sources can be assigned to one of two broad categories, namely renewable and non-renewable energy:

- Also referred to as sustainable or green energy, renewable energy is harvested from self-sustaining environmental energy sources in the proximity (Twidell &Weir, 2006). The field of photovoltaic is the most important among the renewable energy sources because solar energy is omnipresent and bountiful; it is most probably the most important renewable energy source (Bach, 2000).
- Non-renewable energy is finite and is not replenished; over time the reserves dwindle. Because major human intervention, is the energy obtained from static stores of energy that remain under the earth, is involved in recovering these non-renewable resources. Fossil fuels and natural gas are the resources commonly associated with this type of traditional energy. Subsequently, in the twentieth century, the widespread use of nuclear fuel in the commercial development of nuclear energy. Led to its inclusion in this category (Twidell & Weir, 2006).

1.3.1 Solar energy

Not only does the Sun drive climate changes and weather systems, it also radiates vast quantities of solar energy onto the surface of the Earth. The sun provides most of the energy

resource on earth indirectly or directly In addition a lot of this energy is converted into other forms of energy, like for instance Electric power and thermal energy.

With the awareness of limited conventional energy sources and the need for cleaner, sustainable energy sources, a lot of attention has been directed to developing various solar technologies to harness the Sun's energy for both industrial and residential use. These technologies include photovoltaic, air conditioning and refrigeration, and the direct application of the heat energy to heat water, and for drying and cooking.

With the African continent straddling the equator, it receives an abundance of sunshine, with many African countries exposed to daily radiation levels between 5 and 6 kWh/m^2. Notwithstanding this rich source of renewable energy, the number of significant solar projects on this continent is constrained by financial limitations. Despite this limitation, there are a number of African countries which are showing an interest in developing solar energy; one such country is South Africa (Simelane & Abdel-Rahman, 2011).

1.3.1.1 Solar radiation

The Sun is an extremely hot sphere of gaseous matter formed by nuclear fusion at its core; it has a diameter of about 1.39 million km and the average distance between the Earth and the Sun is 149.6 million km. Radiation from the Sun can be categorized as either terrestrial or extraterrestrial (Duffie& Beckman,1980).

The sun is a sphere with a blackbody temperature of approximately 6000Cº (Kane: 2005) which emits radiation. Solar energy is transmitted from the Sun to the Earth as electromagnetic radiation. The total quantity of solar radiation received by a surface at right angles to the transmission direction and located above the Earth's atmosphere, is effectively constant throughout the year and is defined as the solar constant, Isc. The solar constant has a value of about 1367 W/m2 (Gueymard, 2004). Among the components of solar radiation reaching the Earth there is approximately 43% visible light, 37% infrared radiation and 7% UV light.

As shown in figure 1.1, the solar irradiation has a broad energy spectrum which is distributed into wavelengths (Suri et al., 2007).

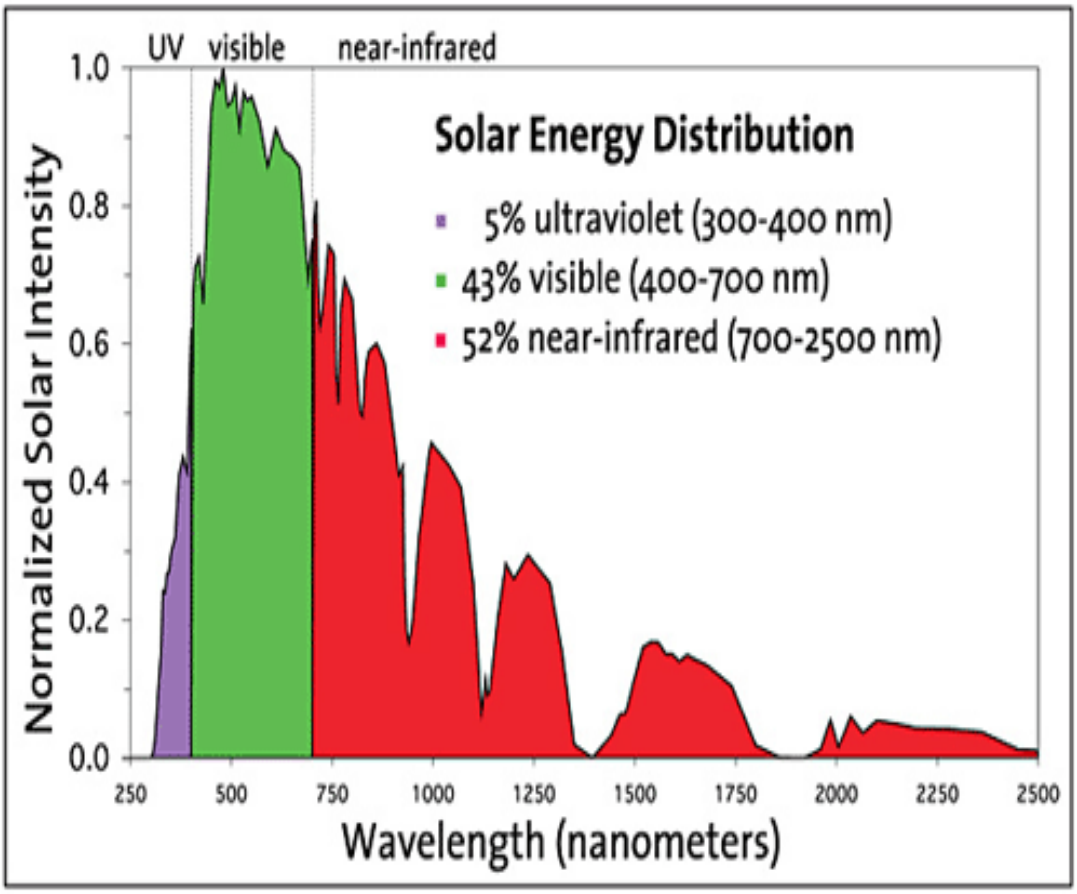

Figure 1-1: The spectrum of solar radiation (Zhang et al., 2012)

Solar energy is transmitted to the Earth's surface through radiation. This radiation is comprised of millions of photons which are high energy particles. Each photon embodies a set amount of energy.

The radiation that the Earth receives from the Sun has differing wavelengths; these wavelengths range from gamma rays and x-rays to ultraviolent (UV) light and radio waves (Badescu, 2008).

The rate at which energy emitted from the Sun is 3.8×10^{23} kW, generated by the conversion of mass to energy at a rate of 4.7×10^{6} ton/s. Notwithstanding the distance of about 150 million km between the Sun and the Earth, about 1.7×10^{17} kW reaches the surface of our planet (Kreith & Krumdieck, 2014).

Because of the elliptical orbit of the Earth around the Sun, the distance between them varies over time (Sonnenenergie, 2008), and this causes the irradiance to fluctuate between 1325W/m2 and 1412W/m2 at the top of the Earth's atmosphere. The average irradiance is 1367 W/m^2 and is termed the solar constant.

The solar constant is the amount of solar energy of all wavelengths received per unit time on unit area of surface perpendicular to the direction of propagation of the radiation at mean earth-sun distance outside the atmosphere (Duffie & Beckman, 2013). The solar spectral irradiance is the spread of this energy over confined spectral bands (Thekaekara & P., 1970).

To determine the solar constant, the product of the irradiance of the surface of the Sun and the radius of the sun squared, is divided by the mean distance between the Sun and the Earth. Irradiance is occasionally called the radiant flux and it is an indication the Sun's emitted electromagnetic energy.

$$I_{SC} = \sigma T = \left(\frac{R}{D}\right)^2 = 1367\ W/m^2$$

Where: I_{sc} = solar constant

$\sigma = 5.67 \times 10^{-8}$ W / $m^2.K^4$ is the Stefan Boltzmann constant.

$R = 696 \times 10^6$ m is the sun radiuses.

$D = 150 \times 10^9$ m is the average distance between the sun and the earth (Duffie & Beckman, 2013).

The availability of solar energy on the surface of the Earth is dependent on the weather conditions at a particular location. To design and evaluate solar energy systems for buildings, it is essential to conversant with the prevailing local solar conditions.

In terms of data, the ideal situation for a specific site would be to have data available which has been continuously recorded over a long period of time. Limited solar radiation networks, particularly in less-developed regions, means that solar information for a particular site will mostly be unavailable.

There is therefore a need for the development of solar radiation models. According to Ahmad and Tiwari (2010) the focus of solar radiation models is on the direct irradiation, because it is this direct component which is of primary interest when designing systems driven by solar energy, for example high intensity solar cells and high-temperature heat engine.

1.3.1.2 Solar heat

Harvesting the sun's energy as heat is comparatively uncomplicated and can be achieved using devices of concentrating, or static installations. The type of installation selected will depend on the end-use temperature level required. Typical heat energy applications are space heating or cooling, water heating, process heat, electricity generation and the manufacturing of fuels. It is substantially cheaper to store heat as opposed to storing

electricity. Coping with the seasonal variation in the solar heat available at an acceptable cost level however, is still a challenge (International Energy Agency IEA, 2011).

1.3.1.3 Solar water heating

Solar radiation is harnessed as an alternative energy source for numerous industrial and domestic applications. Currently, apart from space heating, air-conditioning and lighting ((EIA), 2005).

Under normal conditions domestic water heating can constitute a third of the energy consumed. One of the most profitable applications of solar energy currently is solar water heaters (SWH). SWH constitute the bulk of the current market of solar heating and cooling; which itself produces almost four times more energy than all solar electric technologies combined. Simple systems such as thermo-siphon not protected against freezing, with flat-plate or evacuated tube collectors, can be installed on terraces and horizontal rooftops in mild climates (see Figure 1.2). Integration of pumped systems in buildings facilitates the use of stratified water tanks in which hot water can be stored for several days, with the option of a back-up from another energy source (Shukla, Sumathy, Erickson, & Gong, 2013).

One of the most advantageous solar applications to limit domestic electricity consumption is solar water heating which can contribute of about 70–90% of the total costs of heating water. This increased efficiency and sustainability has come out from developments over the last thirty years, making this form of solar utilization economically viable.

During 2011, the capacity of solar water heating (SWH) systems globally increased from 185 GW thermal at the start of 2010 to 160 GW thermal. Though China leads in SWH market (118 GWth), but there was also a significant expansion of the SWH market in Europe, India, Brazil and Japan. In the United States, however, it has been the relative development of the market regarding the need for solar water heating (Ahmed et al., 2011)

Figure 1-2: solar water heater (http://texasenergyexperts.com/solar-water-heater/)

1.4 Solar water heating systems

Solar water heating systems consist of a collector, an energy transfer medium and a storage facility. Solar radiation is absorbed by the collector and converted to heat. The heat is transferred to the transfer medium which can be water, a liquid which freezes at a low temperature, or air. The transfer medium conveys the heat energy to the point of application or alternatively to a storage unit if the heat is not immediately required. Solar water heating systems are generally low-temperature applications, and because of their simplicity and relative efficiency, these systems are arguably the most commonly used for domestic water heating (Kalogirou, 2014).

For solar water heating there are two systems: an open-loop or direct system in which the water is heated in the collector and circulated to the storage tank, and a closed-loop or indirect system where the heat is transferred to a heat exchanger by a heat transfer medium which is isolated from the water being heated. For both ŧ systems the driving force which circulates the transferring medium can either be a thermo-siphon, a pump, or a fan (Shukla et al., 2013).

These systems can also be broadly categorized as passive solar water heating systems and active solar water heating systems. Passive systems are self-pumping and regulating and require no power input to drive pumps or fans; while active systems usually incorporate one or more circulation pumps and an electronic controller. In a direct system, the potable water is

circulated through the solar collectors to the storage, as opposed to, an indirect system where an intermediate fluid transports heat from the solar collectors to the storage (Shukla et al., 2013).

1.4.1 Passive solar water heating systems

1.4.1.1 Thermo-siphon systems

This system makes use natural forces and does not need a pump. The storage tank must be elevated relative to the collector. During the day when the sun heats the transfer medium in the collector, causing it to expand and become less dense. This less dense transfer medium then rises up the return pipe connected to the top of the storage tank. The rising heated transfer medium causes a partial vacuum in the collector, which is filled by the colder transfer medium at the bottom of the storage tank. In this way the transfer medium continuously circulates in the system (Kudish, Santamaura, & Beaufort, 1985).

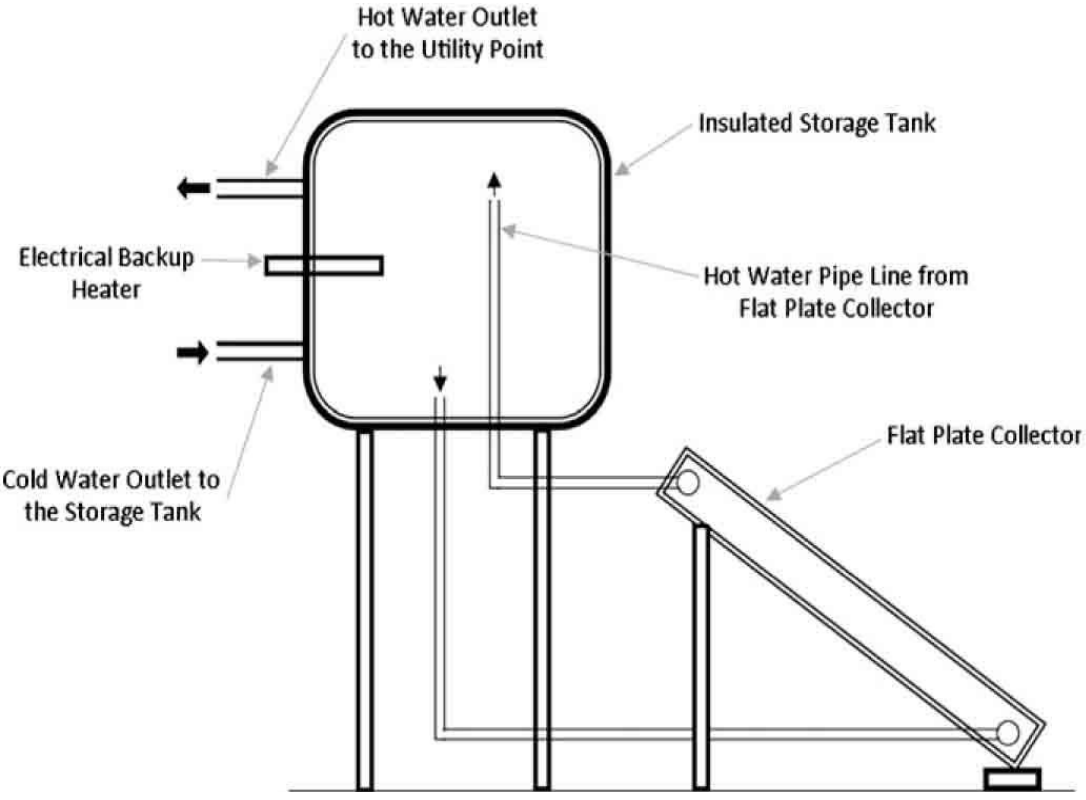

Figure 1-3: Line diagram of a typical thermo-siphon SWH (Shukla et al., 2013)

1.4.1.2 Integrated collector storage systems

In integrated collector storage (ICS) system the collector and storage facility constitute a single unit, with surface of the storage tank acting as a collector. Using the principle of the thermo-siphon action in the storage tank, hot water is drawn from the top of the tank where

the temperature is highest, and the cold water supply feeds into the bottom of the tank (Smyth, Eames, & Norton, 2006).

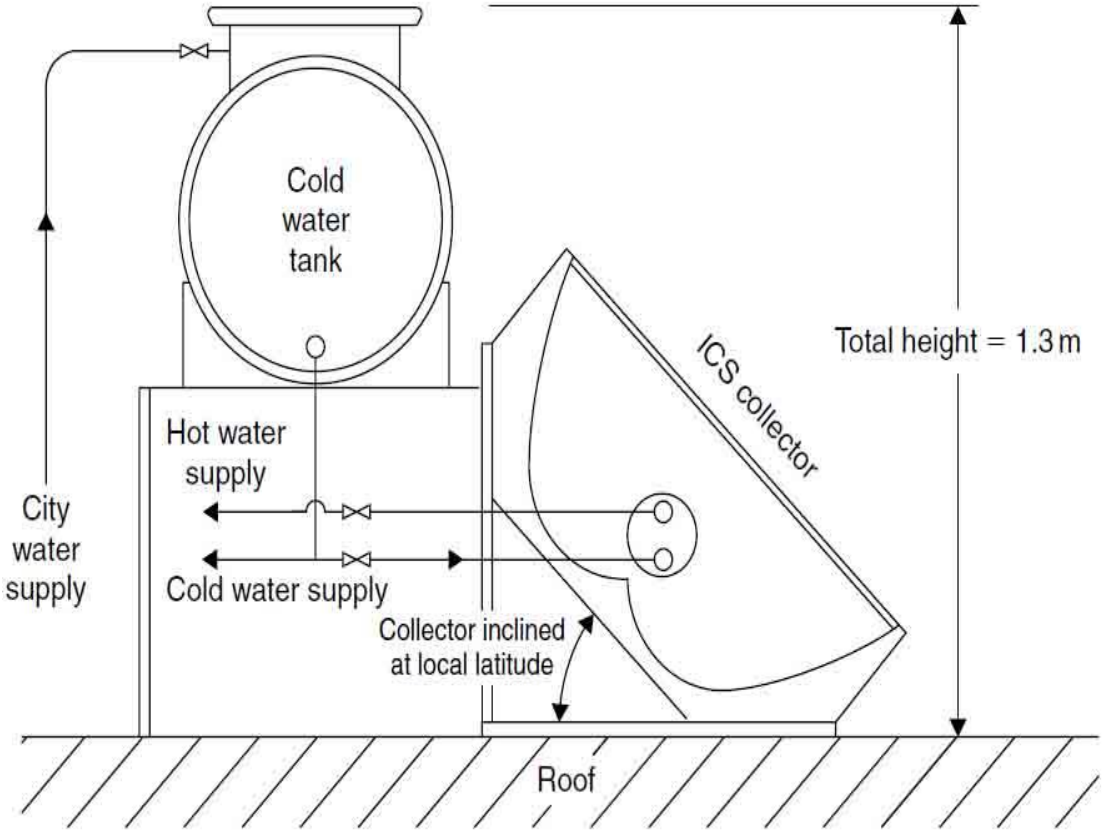

Figure 1-4: Integrated Collector Storage System (Kalogirou, 2014)

1.4.2 Active solar water heating systems

There are a number of Active solar water heating systems: direct circulation systems, indirect water-heating systems, air systems, heat pump systems and pool heating systems. All these systems include various thermostatic options to control the operation of the pumps or fans, as well as collector drainage facilities to protect the collector against cold-weather conditions (Kalogirou, 2014).

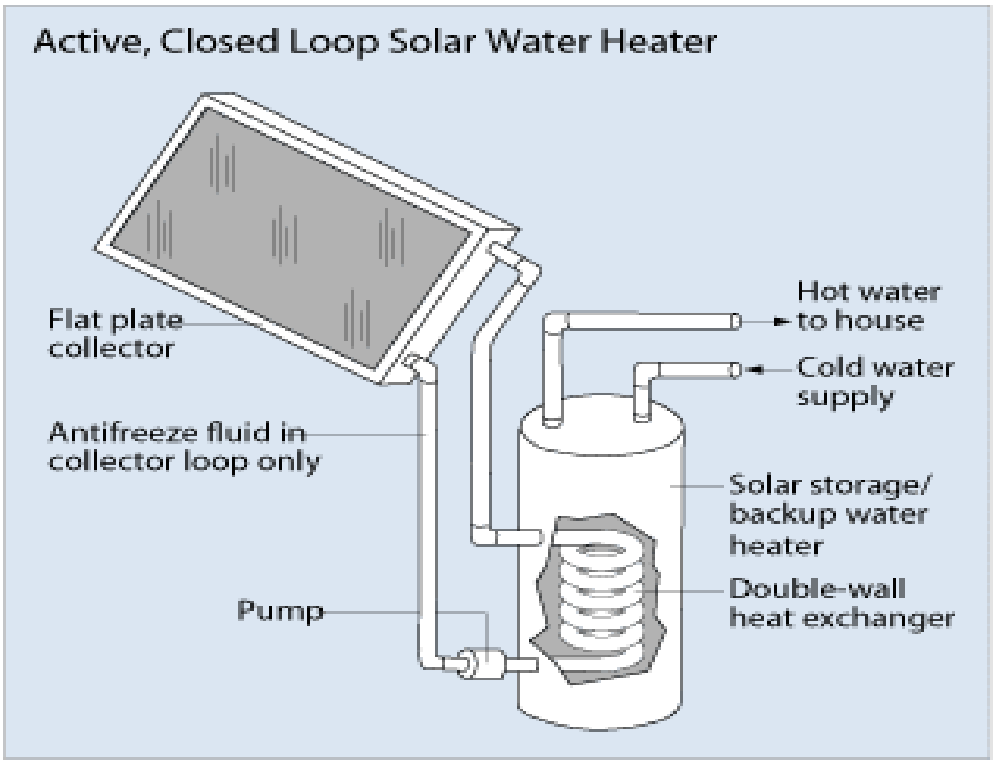

Figure 1-5: Active solar water heating system (En, 1996)

1.4.2.1 Direct circulation systems

Since the driving force for the flow of the transfer medium is provided by a pump, there are no requirements regarding the elevation of the storage tank relative to the collector. The pump is usually controlled by a thermostat that operates when the collector outlet temperature is a predetermined temperature higher than the water in the storage tank. The storage water itself forms the transfer medium (Raisul Islam, Sumathy, & Ullah Khan, 2013).

1.4.2.2 Indirect water-heating systems

This type of system is similar to a direct circulation system in that it is also driven by a thermostatically controlled pump and the relative elevations of the components do not matter. For this type of system however, the transfer medium is a specific fluid, isolated from the water being heated. This has the advantage that a transfer fluid with a low freezing point can be selected, allowing the system to operate at below-zero temperatures; a fluid like a water-ethylene glycol is typically used. The transfer medium flows through the collector picking up heat, and is pumped through coils or a manifolds which is in contact with the water in the storage tank (Patel, Patel, & Patel, 2012).

1.4.2.3 Air water heating systems

Air systems make use of air as the heat transfer medium. A fan forces the heated air from the collector, via ducting, to a heat exchanger where the heat is transferred to the water being heated, where after the cooled air is circulated back to the inlet of the collector. Water reticulation between the storage tank and the heat exchanger is a separate, pump-driven subsystem, circulating the water to be heated, through a coil or a mantle in the heat exchanger and back to the storage tank (Raisul Islam et al., 2013).

1.4.2.4 Heat pump systems

Heat pumps make of the mechanical-compression cycle to extract heat from ambient air and then convey this heat to a heat sink, this heat sink then effectively becomes a heat exchanger when water from a storage source is pumped through it in an isolated piping system, similar to the subsystem described for air systems above. The efficiency of heat pumps is very high (Hepbasli & Kalinci, 2009).

1.4.2.5 Pool heating systems

These systems operate in the same way as direct circulation systems, utilising the pool pump to drive circulation and using the pool itself as the water storage tank. Water is pumped from the pool and pushed through a network of black plastic pipes exposed to the Sun, and then returned to the pool (Kalogirou, 2014).

1.5 Problem statement

1.5.1 Purpose

The purpose of this experimental research is to decouple TCO coating from the absorber to avoid inter-diffusion and then test by optical simulations and measurements of optical properties, the enhancement or degradation of spectral selectivity performance of the TCO coating in high temperature solar selective absorbers.

1.5.2 Research objectives

The objectives of this research are to:

- simulate numerically the absorbance and emissivity performance of transparent conducing oxides (TCOs) as function film thickness,
- build a physical model micro solar concentrator, based on transparent conducting oxides,
- Validate the simulated data and compare the efficiency with a similar model based on classical technology.

1.6 Research methodology

The research methodology involves a comparison of the thermal efficiency of two models. The first model parabola without glass while the second model is covered with a glass sheet coated with textured TCO based on selective absorbers.

TCOs are electrically conductive materials with comparatively low absorption of electromagnetic waves within the visible region of the spectrum. They are usually prepared using thin-film technologies and used in optoelectronic applications such as solar cells (Stadler, 2012).

In the first model without glass, water circulating in copper tubing absorbs the transmitted solar heat, causing a rise in the temperature inside the model up to a maximum. At this maximum point a balance is reached where the heat lost, equals the incoming heat from the sun. In the second model with the textured TCO coated glass, any heat is covered with a glass sheet coated with textured TCO; any heat directed at the underside of this glass will be not be transmitted externally, but instead will be reflected and thus retained within the enclosure. Under similar solar exposure conditions, the maximum temperature within the second model should therefore be significantly higher for the second model In comparison to the first model, this will result in a substantially higher maximum temperature inside the second model.

1.7 Data analysis

All collected information will be analyzed using Spreadsheet application or Excel solver to give us good incite on the depth of the efficiency of two models and to highlight the statistical analysis using graphical component of pie chart or clustered column chart.

1.8 Facilities

This research project will be conducted in the mechanical engineering department faculty of CPUT and it will deal with modeling thermal efficiency and spectral features of both models. On the practical side, micro solar collectors based on both models will be built to validate the simulated results.

CHAPTER TWO

LITERATURE REVIEW

2.1 Introduction

Renewable energy is obtained from clean sources of energy; the five sources generally acknowledged as providing clean energy are biomass, wind, solar, hydro and geothermal energy. At this stage there are many applications where renewable energy has been shown to be a cost-effective solution; there are however, still many obstacles limiting the implementation of renewable energy installations. Once these obstacles are overcome, this form of energy will potentially substantially expand its contribution to the total energy supply of the world. There are still huge numbers of people in rural, isolated areas, particularly in lower-income countries, to whom clean energy is not available. The economics associated with the provision of clean energy is already big business in terms of money invested and job creation, and with the growth of this sector, these numbers are set to increase. Countries investing in the development, manufacture, installation and export of innovative sustainable energy technologies, according to Painuly (2001), are likely to reap the economic benefits going forward.

Energy conversion systems for harnessing solar energy with specific reference to generating electricity, heating water, and space heating and cooling, are considered; for each of these systems the fundamentals and utilization of the solar energy are discussed. The processes of solar radiation and procedures for assessing radiation data are deliberated prior to a discussion of the varied ways in which solar energy systems are practically used. The basics of heat transfer, the thermodynamic laws, and optics are utilized to clarify the thermal energy conversion in a solar system (Painuly, 2001).

In solar water heating systems, solar collectors are considered the most important element in the composition of heating system. The types of collectors reviewed include Flat plate collectors, tube-type collectors, concentrating collectors, collectors that are intermittently adjusted or fixed, and concentrators capable of tracking. Also reviewed are processes for evaluating solar energy systems, their components and their viability.

Thermal facets and the engineering of systems for solar water heating are assessed. Also briefly reviewed are the fundamentals of the components related to electricity generation from solar energy, like industrial heat processing, distillation, photovoltaic panels, and solar storage ponds (Kreith & Kreider, 1978).

2.2 Solar collectors

A solar thermal collector is a device for capturing solar radiation by absorbing sunlight. Solar energy is derived from a particular part of the electromagnetic radiation emanating from the sun; solar energy comes mainly from the electromagnetic radiation which ranges from infrared waves, through the visible light spectrum, to ultraviolet waves. The quantity of energy which reaches the surface of the Earth depends on the cloud cover, the geographic location, and the orientation relative to the incoming rays.

'Solar collector' is a term which usually refers to solar hot water panels. The term may however, also refer solar components like air heaters, parabolic troughs, or even central tower power plants. Concentrating solar power installations employ mirrors or lenses to concentrate a large area of sunlight, and the heat collected then drives a heat engine which in turn is used to generate electricity. To heat internal spaces in buildings, simple collectors are commonly used (Norton, 2014).

The harvested solar energy is then transported by the circulating medium to either directly to a space heating plant, or a water heating plant; alternatively, it is stored in a thermal energy storage unit, from where it can be retrieved at a later stage when heating is needed. Essentially there are two sorts of solar collector; they are stationary or non-concentrating collectors, and concentrating collectors (Kalogirou, 2004).

2.2.1 Solar collector types:

2.2.1.1 Non-concentrating collectors

The area intercepting the solar rays is called the collector area, and the actual area of the collector is called the absorber area. For non-concentrating collectors, the collector area and the absorber area are the same. Of the non-concentrating collectors, the most widely used collectors are the flat plate type and are used when temperatures lower than 93.3°C are sufficient. When air or water has to be heated for swimming pools, or for the internal spaces in buildings, non-concentrating collectors are frequently chosen. Although there are a multitude of flat plate collectors, their design mostly includes distinct parts, but they generally have four specific components (Kalogirou, 2004):

- The incident solar radiation is intercepted and absorbed the solar energy by a flat plate absorber
- A transparent cover that allows solar energy to pass through, but reduces heat loss from the absorber

- A heat-transport fluid (air or liquid) flowing through tubes to remove heat from the absorber
- A layer of insulation on the back of the absorber

2.2.1.2 Concentrating collectors

Concentrating collectors intercept a substantially larger area of solar radiation than the area of the absorber. The solar energy picked up by the collector is intensified when it is transmitted to the absorber. To boost their efficiency, collectors are usually capable of being orientated so that they maintain a high level of absorber (Kalogirou, 2004).

As mentioned, the intercepting area and the absorber area for a non-concentrating collector are the same; a concentrating collector which tracks the Sun, often consists of a large concave mirror which reflects and raises the solar flux by concentrating the solar energy onto a smaller absorber. There are many commercially available solar collectors. A survey of the different types of solar collector will be set out in this section.

Solar collectors are specifically designed to harvest solar energy in the form of heat, which can then be applied an energy source. Solar collectors are categorised according to their concentration ratio, C, where: In concentrating solar power (CSP) systems like central towers, the parabolic dishes, and the parabolic troughs, the concentration ratio is above one; in non-concentrating collectors like evacuated tube collectors and flat plate collectors, the concentration ratio is one. The concentration ratio depends on geometric characteristics, and it is given by:

$$\mathrm{C} = \frac{A_a}{A_\gamma} \qquad (2\text{-}1)$$

With: A_a the area of the collector, and

A_γ the energy absorber

The geometric concentration ratio is a measure of the average concentration for the case where energy flux in the receiver is homogeneous, although this is not what actually happens. In practice the spread of the flux is more complicated, belying the assumption of

A uniform distribution; the intensity at the center of a receiver is generally high and it then falls off toward the edges (Sen, 2008). Depending on the working temperature range capabilities of the materials used in the construction of a solar collector, it can be classified as: a low-temperature collector if it operates below 100°C; a mid-temperature collector if it operates between 100 and 400°C, and; a high-temperature collector if it operates above 400°C.

Typically CSP installations use mid- or high-temperature collectors, while flat plate collectors are low-temperature collectors (Kennedy, 2002)(Nuru, 2013).

2.3 Concentrated solar thermal systems

A solar collector acts as a heat exchanger, converting solar radiation into heat energy which can in turn be applied to generate power. A solar collector takes up incoming solar radiation and transforms it into thermal energy; this thermal energy is then transferred to a flowing, heat transfer fluid (HTF) that is in thermal contact with the collector. The heat is then piped, either to a system generating power, or to a thermal storage facility (Barlev et al., 2011).

Solar radiation collectors can be assigned to one of two broad groups; firstly, the non-concentrating type which is generally stationary, where the collection and absorption of solar energy is effected on the same area.

Concentrating collectors form the second group; these solar collectors mostly incorporate mechanisms to track of the Sun, thereby optimizing the harvesting of available solar radiation; additionally, these collectors make use of reflectors and/or lenses to concentrate the solar energy intercepted, onto a smaller absorbing area.

According to Barlev et al. (2011) the mean incoming solar energy on the surface of the Earth is measured in suns, where one sun is equivalent to 1000 W/m2 Another concept applicable to concentrating collectors is the sunlight concentration ratio, which is the area of a collector divided by the focus area onto which the sunlight is beamed.

The higher costs of concentrating collectors have numerous advantages over stationary collectors; the main benefits being that they operate at a higher temperature and are more efficient (Kalogirou, 2004).

Adding an optical device increases thermodynamic efficiency by increasing the quantity of heat collected from a set area, in addition to yielding a higher operating temperature. Concentrating the solar radiation means that receivers with relatively small surface areas can be used, leading to a substantial reduction in convection heat loss. Notwithstanding the extra expense needed to produce the optical components of the equipment, the materials used for these mirrors/lenses are generally inexpensive compared with thermal collector materials; the extra capital is therefore partly offset by the smaller collector area required for the concentrator setup (Barlev, Vidu, & Stroeve, 2011).

With the reduction in receiver size and correspondingly the amount of materials required, it makes economic sense to improve efficiency and limit heat loss by enhancing receiver function by means of technology like vacuum insulation and surface treatments, despite these

treatments being expensive. With concentrating solar collectors, subtle adjustment of the operating temperature is possible by controlling the concentration ratio of a system; to prevent energy waste, the operating temperature can be matched to the thermodynamic requirements of a specific application, as required. With regard to the cost-effectiveness of reflective materials used in CSP technologies, Barlev et al.(2011) noted the importance of these materials meeting specific reflectivity and lifespan standards.

There are four main types of concentrating solar collectors: parabolic trough collectors (PTCs), parabolic dish collectors (PDCs), heliostat field collectors (HFCs), and linear Fresnel reflectors (LFRs). These collectors are briefly discussed in the sub-sections which follow.

2.3.1 Parabolic trough collectors

A linear parabolic trough collector is most often incorporated in a CSP system; as shown in Figure (2.1), the absorber tube is located along the focal line of the parabolic reflector and fixed to the trough collector frame. The tube (solar field piping) is fixed to the mirror structure, and the heated fluid either a heat-transfer fluid or water/steam flows through and out of the field of solar pipes to where it is used to create steam (Bakos, Adamopoulos, Soursos, & Tsagas, 1999). In the situation where the heat has to be delivered at a water or steam receiver, the heat is taken to the turbine directly (Nuru, 2013).

With most industrial processes requiring heat the great majority of which run below 300 ºC. This makes parabolic trough collectors, effectively produce heat at temperatures ranging from 50 to 400 ºC; these temperatures are generally high enough for most industrial heating processes and applications.

PTCs are comparatively efficient. A parabolic trough collector comprises parabolic-shaped reflective sheets which are fixed side-by-side to form a reflective parabolic trough; these sheets are often made of usually silvered acrylic. These modules are supported from the ground by simple pedestals at both ends.

A parabolic trough collector has a focal point in section, which the length of the reflector; it is on this line that the collector tube which absorbs the concentrated heat, is mounted. To improve the efficiency of heat absorption by the metal collector tube, it is commonly painted black, using a special selective coating which has high heat absorption and low heat emission properties. Also, the collector tube can be run inside a glass tube for the length of the reflector; this will restrict the loss of heat resulting from convection. To further enhance heat transmission, an antireflective coating can be applied to glass tube, and a partial vacuum can be created (Barlev et al., 2011).

A PTC can be mounted with it longitudinal in an east–west direction, and then rotated north-south to track the seasonal inclination of the rays of the Sun. An advantage of this setup is that the daily adjustments are small because there is a six-month period between the extreme positions of the Sun. However, the full aperture only faces the Sun at noon, while the while early mornings and late afternoons the angle of incidence of the Sun low, resulting in very inefficient heat collection.

Alternatively, the longitudinal axis can be placed in a north-south direction, and adjusted east-west to track the diurnal movement of the Sun. For troughs placed north–south, the ir highest cosine loss occurs at midday and the lowest loss occur during early mornings when the Sun is directly east, or late afternoons when the Sun is directly west.

Over a year, a PTC with its horizontal axis in a north–south direction will usually gather marginally more heat energy that the same PTC placed in an east–west direction. In the north-south orientation however, a lot more heat is collected in summer than in winter. This is in contrast to the east–west orientation, in which slightly more heat is collected during winter than in summer. The selected orientation would therefore depend on the application and desirability of more energy in the summer than in the winter.

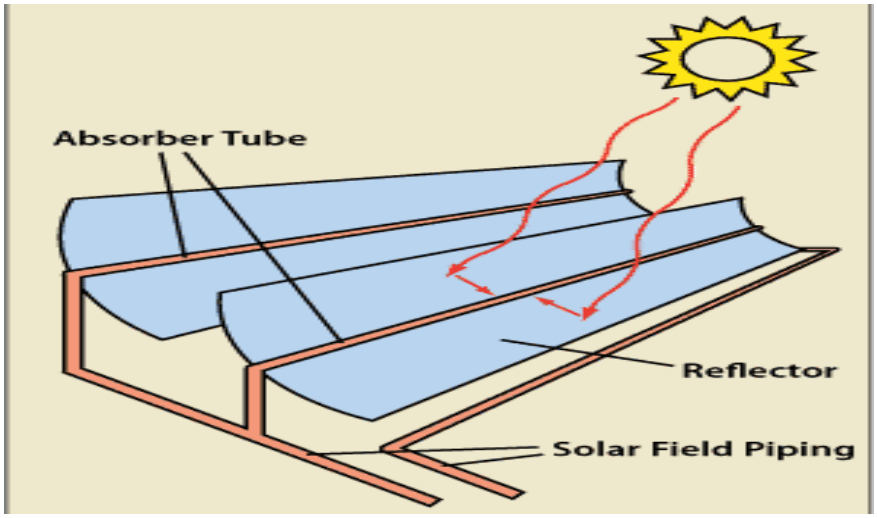

Figure 2-1: Schematic of a parabolic trough system figure from (Nuru, 2013)

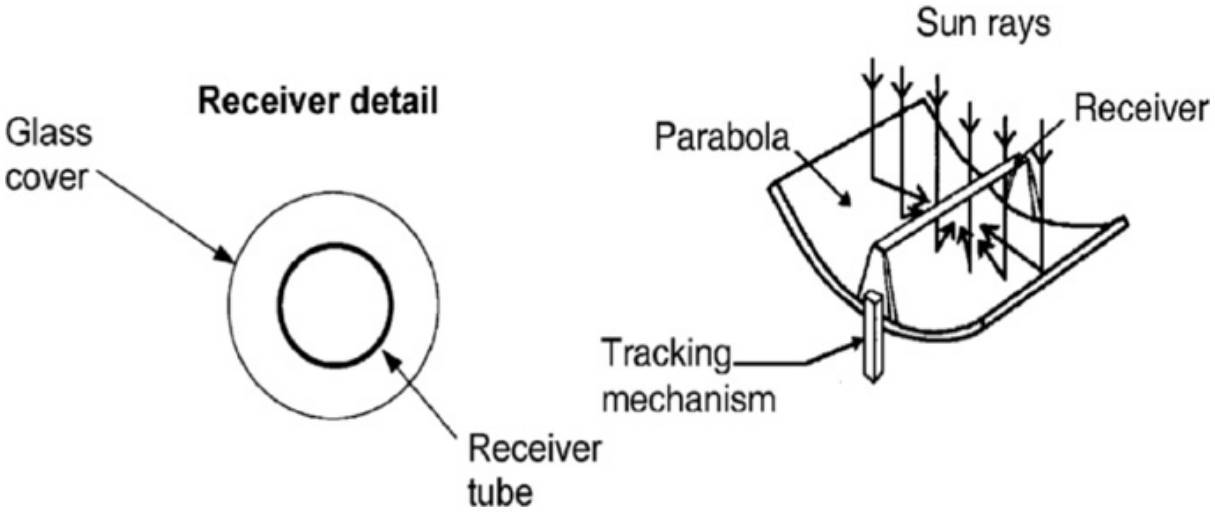

Figure 2-2: Schematic of a parabolic trough collector from (Kalogirou, 2004)

2.3.2 Parabolic dish collectors

According to Foster et al. (2010), parabolic dish systems deliver the highest level of energy. Such systems consist of dish-shaped reflective parabolic collectors which concentrate the rays of the Sun at its focal point, where a receiver is mounted to absorb the reflected solar energy see Figure (2.3). This system works by collecting and concentrating the sun's energy with a dish shaped surface onto a receiver that absorbs the energy and transfers it to the engine. The engine then converts that energy to heat. Which is then converted to mechanical power; this conversion to mechanical power is effected by compressing the working fluid when it is cold, heating the compressed working fluid, and then expanding it through a turbine or with a piston to produce mechanical power. The mechanical power is then applied to a generator which outputs electrical energy (Foster, Cota, & Group, 2010).

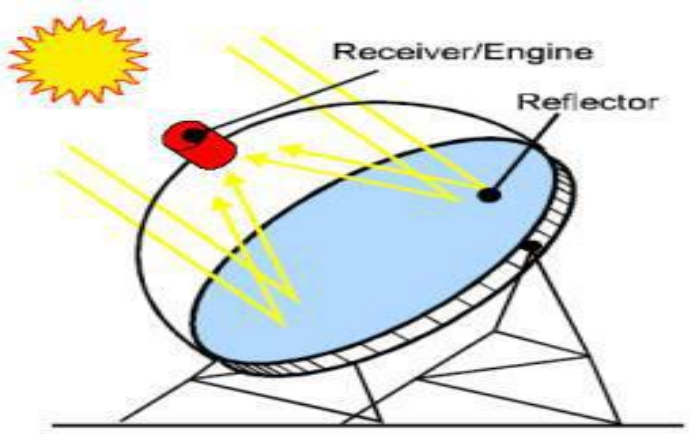

Figure2-3: Schematic of solar dish system (Nuru, 2013)

2.3.3 Heliostat field collectors

Power towers or central receivers consist of a heat receiver located at the top of a tower, and at ground level there is a conventional steam-driven electricity plant. Heat is reflected onto the receiver from by a large number of mirrors placed around the base of the tower, which reflect the light and heat from the Sun onto the heat receiver; these mirrors are referred to as heliostats (see Figure 2.4). The reflected heat from the heliostats is transferred the molten salt transfer fluid which circulates and conveys the heat to the base of the tower, where it generates steam for driving the conventional generation of electricity via steam turbines (Nuru, 2013).

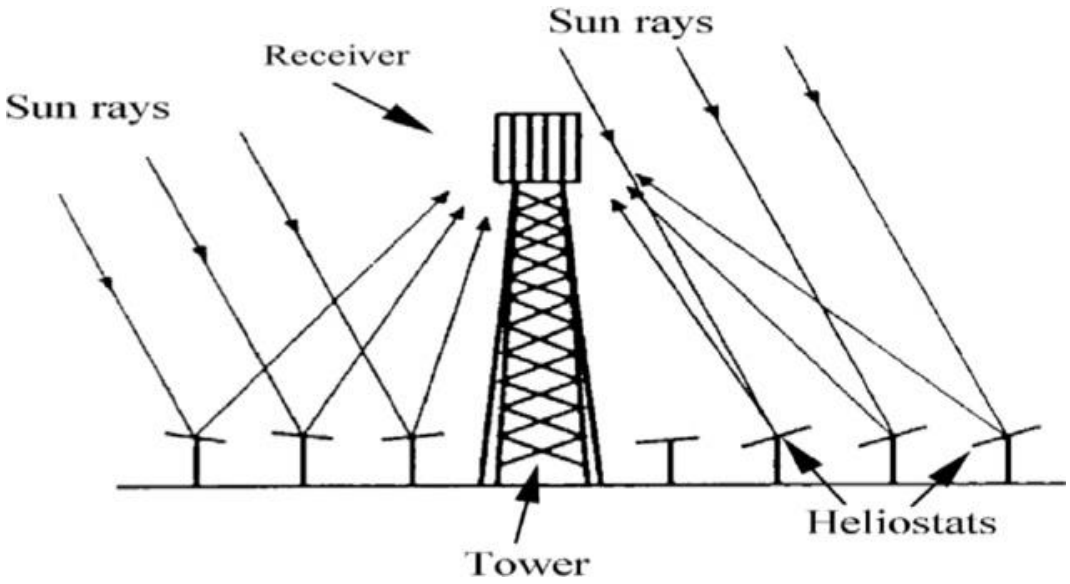

Figure2-4: Schematic of a central receiver system (Kalogirou, 2004)

2.3.4 Linear Fresnel reflectors (LFR)

LFR design is significantly cheaper than PTC. The operating principals and configuration of LFRs and PTCs are similar. LFRs consist of linear arrays of flat mirrors, adjusted to reflect the rays of the Sun onto a horizontal, longitudinal receiver that is mounted about 10–15 m tall, suspended above and along reflector arrays. The mirrors can be mounted on one or two-axis tracking devices, because of their flexible nature see Figure (2.5).

Furthermore, the relatively small receiver effects a saving because receiver materials are usually bigger than the cost of reflector materials. For an LFC system, several banks of suitably adjusted flat mirrors can be arranged to simulate the shape of a parabolic trough.

Another advantage of LFRs is that the stand-alone receiver does not need to be supported by the tracking devices, unlike the arrangement for PTCs; this increase efficiency of tracking in LFR systems. The solar energy absorbed by the receiver is transferred to a fluid circulating through the receiver

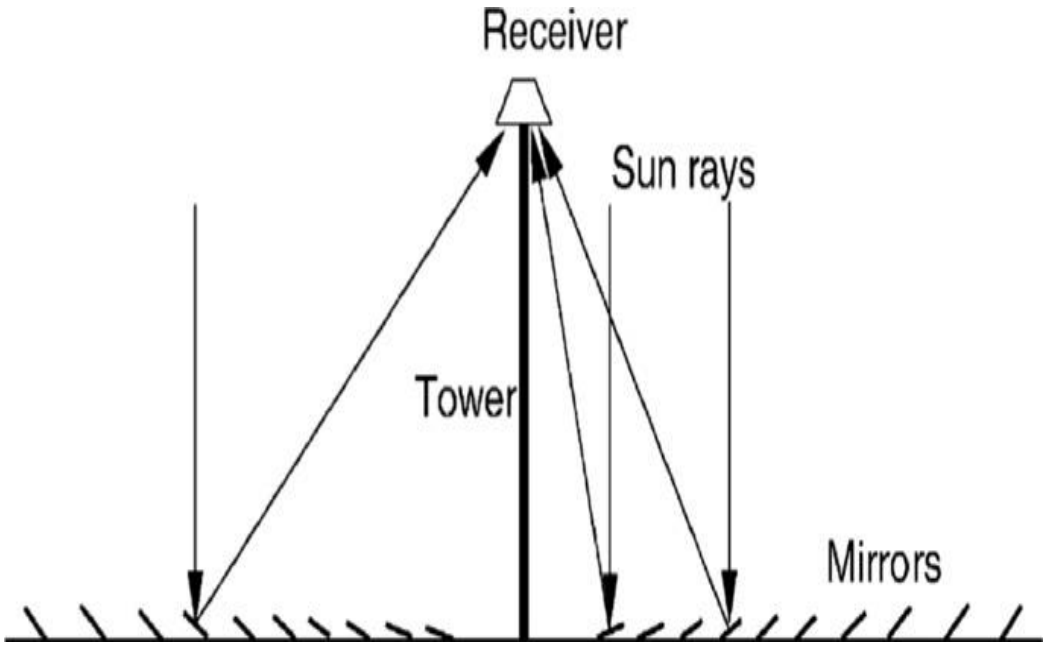

Figure -6: Schematic diagram of the LFR design (Barlev et al., 2011)

Error! No text of specified style in document.

Table 2-1: Description and specifications of the four main CSP technologies (Barlev et al., 2011).

	Description	Relative. thermodynamic efficiency	Operating temp. range (ºC)	Relative cost	Concentration ratio (sun)	Technology maturity	Tracking
PTC	–parabolic sheet of reflective material (aluminium, acrylic) –Linear receiver (metal pipe with heat transfer fluid)	Low	50–400	Low	15–45	Very mature	One-axis

Linear Fresnel	–Linear Fresnel mirror array focused on tower or high-mounted pipe as receiver Low	Low	50–300	Very low	10–40	Mature	One-axis
Solar tower	– Large heliostat field with tall tower in its center – Receiver: water/HTC boiler at top – Can be used for continuous thermal storage	High	300–2000	High	150–1500	Most recent	Two-axis
Dish-Stirling	– Large reflective parabolic dish with Stirling engine receiver at focal point – Can be used with/out HTC, if heat engine produces electricity directly from reflected thermal energy (in this case, thermal storage cannot be achieved by the system)	High	150–1500	Very high	100–1000	Recent	Two-axis

2.4 Transport of energy by radiation

There are three transport mechanisms for the transfer of thermal energy: conductive, convective, and radiative (Geankoplis, 1993). Radiative energy transport, unlike conductive and convective energy transport does not require the presence of a material medium (Welty, Wicks, Wilson, & Rorrer, 2008). In fact, heat conduction relies on a temperature difference between neighboring regions of a solid material while heat conduction require a fluid that is free to move around, transporting energy with it (Bergman, Lavine, Incropera, & DeWitt, 2011). Radiation on the other hand allows the transport of energy within regions of space devoid matter (Halliday, Resnick, & Walker, 2011). It is an electromagnetic phenomenon which permit the transport of energy through those regions with the speed of light (Bird, Stewart, & Lightfoot, 2002). A complete understanding of the physics behind radiative transport calls for the knowledge of concept from several disciplines. In fact, electromagnetic theory explains the wavelike nature of radiation; thermodynamics allows the determination of correlations among bulk properties of an enclosure containing radiation; quantum mechanics gives a detailed understanding of the atomic and molecular processes occurring during radiative processes; statistical mechanics plays a crucial role in explaining the distribution of radiative energy over the wavelength spectrum (Bird et al., 2002). The discussion which will

follow in this chapter will introduce and define the concepts required for the understanding of radiative energy transport.

2.5 Fundamental concepts

Supplying energy to the constituent molecules and atoms of a solid body raise them to an excited state (Kotz, Treichel, & Townsend, 2012). When that happens, atoms and molecules tend to spontaneously lower their energy states (Kotz et al., 2012). The excess energy released is emitted in the form of electromagnetic radiation (Holman, 2010). This phenomenon is known as emission of radiant energy and is characterized by the return of the molecular or atomic systems from a high to a low energy state (Bird et al., 2002). Emission of radiation is the result of changes in the electronic, vibrational, and rotational states of the atoms and molecules. Because of that radiation is distributed over a range of wavelengths (Atkins & Paula, 2010). As indicated by the name, the wavelength is the distance separating two successive high points of a wave or the distance between two low points (Brown, LEMay, Bursten, Murphy, & Woodward, 2012). Thus there are various kinds of radiation distinguished from each other by the range of wavelengths included (Brown et al., 2012). Also, the different forms of radiant energy travel with the speed of light when under vacuum (Silbey, Alberty, & Bawendi, 2005). Hence, the wavelength λ is related the frequency ν of the wave by the expression:

$$\lambda = \frac{c}{\nu} \qquad (2\text{-}2$$

Where c = the speed of propagation in a medium is related to the speed of light by

$$c = \frac{c_0}{n} \qquad (2\text{-}3$$

.c_0 = 2.998x10^8 m/s is the speed of light under vacuum and n is the index of refraction of the medium (Cengel, 2006). For air and most gases, the refractive index can be taken as 1. Glass has a refractive index of 1.5 and water 1.33 (Bergman et al., 2011).

For convenience's sake, electromagnetic radiation can be initially considered from a corpuscular point of view i.e. associating an electromagnetic wave of frequency ν with a photon (Giancoli, 2005). The energy of the corresponding photon is given by:

$$\varepsilon = h\nu \qquad (2\text{-}4)$$

In equation (2-4), h = 6.626x10^{-34} J.s is the Planck's constant (Holman, 2010). Equations(2-2) and (2-4) can be combined into the following correlation:

$$\varepsilon = \frac{h\nu}{\lambda} \qquad (2\text{-}5)$$

Equation (2-) shows that the energy associated with a photon increases with a decrease in the wavelength of the electromagnetic radiation. In other word, the shorter the wavelength of the electromagnetic radiation, the larger the energy released during emission of radiant energy (Serway & Jewett Jr., 2010). It's only logical to conclude from the forgoing statement that the wavelengths of the radiant energy emitted from heated objects, will tend to become shorter as the temperature of the body is raised (Silbey et al., 2005). In fact, when heating a piece of metal, its color turns to dull red at lower temperature. When the temperature is increased further the color brightens, and at higher temperatures the metal starts to emit a brilliant white light (Petela, 2010). What the eyes detect are the radiation emitted in the visible region of the electromagnetic spectrum (Nellis & Klein, 2009). Hidden from the eyes are the ultraviolet and infrared radiation also given off by the hot metal (Nellis & Klein, 2009). In fact, the description of the total spectrum of electromagnetic radiation, given in fig 2-6, clearly shows that visible light constitutes a very small portion of the entire spectrum.**Error! Reference source not found.**

Figure2-6: Electromagnetic spectrum (Kotz et al., 2012)

It should be mentioned that the different types of electromagnetic radiation are produced through a wide variety of mechanism as depicted in 2-7

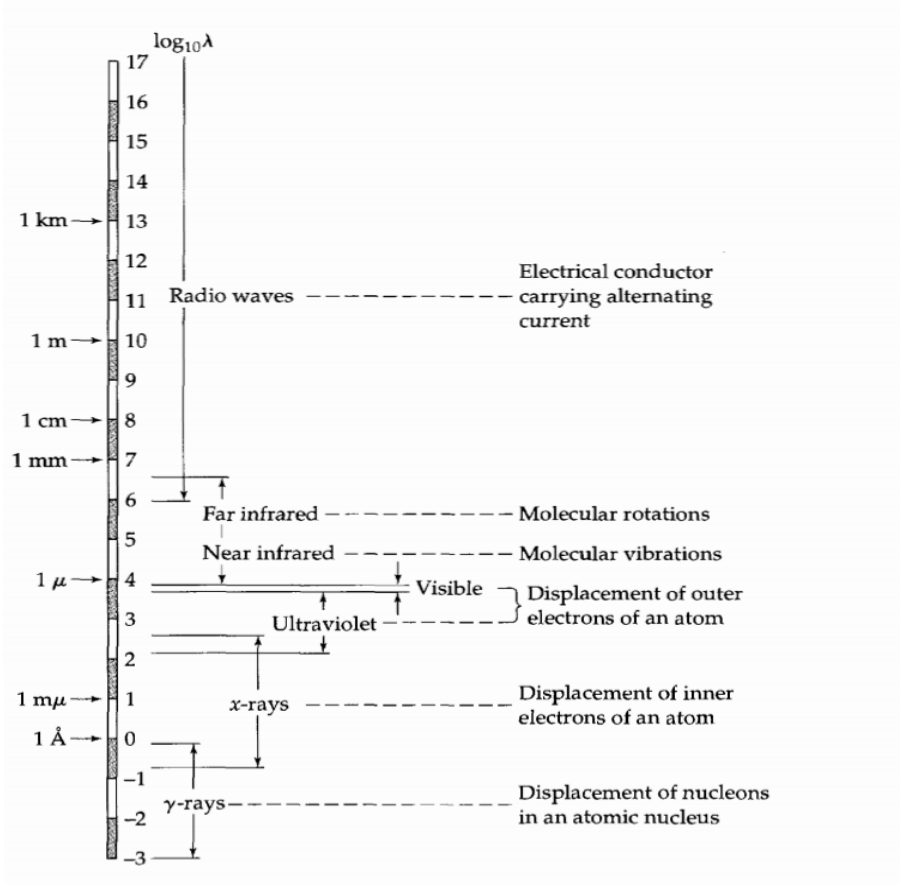

Figure2-7: Electromagnetic spectrum and mechanisms responsible for the various wavelengths of radiation (Bird et al., 2002)

It also happens that addition of radiant energy to a molecular or atomic system causes an increases in energy state (Bird et al., 2002). This process is known as absorption and is the reverse of emission described previously (Bird et al., 2002). During absorption, the radiant energy tend to impinge on a solid surface causing a rise in temperature (Modest, 2014).

1.6 Thermal radiation

The previous section established that there are more than one mechanism responsible for the different types of electromagnetic radiation. The waves of those radiation share the same general feature but nevertheless waves of different wavelength do not behave the same way (Matzler, 2006). The preceding also introduced the concept of electromagnetic spectrum which encompasses a wide range of radiation going γ-rays all the way to long radio waves. Thermal radiation is the only type of electromagnetic radiation which plays a role in heat transfer (Cengel, 2006). Thermal radiation can be defined as the radiation emitted as a result

of the change in temperature of a substance (Kreith, Manglik, & Bohn, 2011). Temperature is a measure of the strength of the energy transitions of molecules, atoms, and electrons of a substance (Levine, 2002). The rate of emission of thermal radiation is known to increase with increasing temperature (Silbey et al., 2005). All matter, whose temperature is above absolute zero, continuously emit and absorb thermal radiation (Atkins & Paula, 2010).

Another definition of thermal radiation is that it is the portion of the electromagnetic spectrum extending from 0.1 to 100 μm (Cengel, 2006). That range more or less encompasses all the radiation emitted by bodies due to their temperature (Cengel, 2006). This means that infrared (IR) radiation and a part of ultraviolet (UV) radiation are a form of thermal radiation (Holman, 2010). Even light also falls under the definition of thermal radiation (Cengel, 2006).

Light is basically the visible portion of the electromagnetic spectrum whose wavelength lie between 0.4 and 0.76 μm (Hollands, 2004). Light is electromagnetic radiation just like any other, expect that it triggers the sensation of seeing in the human eye (Hottel et al., 2008).

When a body emits radiation in the visible range it is termed light source (Petela, 2010). The principal light source of the earth is the sun. Most of the solar radiation (electromagnetic radiation emitted by sun) have a wavelength band of 0.3 - 3 μm (Duffie & Beckman, 2013). Solar radiations are basically half-light and the remaining distributed between infrared and ultraviolet (Duffie & Beckman, 2013). Due to nature of this thesis, the discussion in the remaining part of this chapter will be limited to thermal radiation since it is the only type of electromagnetic radiation relevant to heat transfer.

The electrons, atoms, and molecules of solids, liquids, and gases are constantly in motion and consequently emit and absorb radiation continuously over their entire volume (Brewster, 1992). This means that radiation is volumetric phenomenon (Welty et al., 2008). However, in opaque or nontransparent solids the radiation emitted by the inner regions never reach surface and are absorbed by the molecules closest to the surface (Geankoplis, 1993). Thus for such bodies, only these molecules closest to the surface emit radiations which make out to the surrounding, and the incident radiation is usually absorbed within a few microns from the surface (Cengel, 2006). Thus radiation is considered a surface phenomenon when it comes to opaque solids. A very important thing to note is that it is possible to significantly alter the radiation characteristics of surfaces by applying thin layers of coating on them (Cengel, 2006).

1.7 Blackbody radiation: Stefan-Boltzmann law, Planck's distribution law, and Wien's displacement law

A blackbody is an idealized body able to absorb all incident radiation of any wavelength and coming from any direction (Atkins & Paula, 2010). It also possess the able to emit radiation

uniformly in all directions per unit area normal to direction of emission (Incropera, DeWitt, Bergman, & Lavine, 2007). In order word, a black body is a perfect emitter and absorber of radiation and no surface can emit more energy than a black at a specified wavelength and temperature (Holman, 2010). In 1879 Joseph Stefan determined that the radiation energy emitted by a blackbody per unit time and per unit surface area was proportional to the fourth power of the absolute temperature of that body (Cengel, 2006). The relation was later theoretically confirmed in 1884 by Ludwig Boltzmann and came to be known as the Stefan-Boltzmann law (Cengel, 2006). The law reads as:

$$\mathrm{E}_b(\mathrm{T}) = \sigma T^4 \qquad (2\text{-}6)$$

Where:

$\sigma = 5.67\times10^{-8}$ W/m^2.K^4 is the Stefan-Boltzmann constant

T the absolute temperature

E_b the blackbody emissive power.

It is true that a blackbody would appear black to the human eye but it is not to be confused with an ordinary black surface (Nellis & Klein, 2009). The human eye is relatively easy to trick. When a surface absorbs the visible portion of radiation it appears black and when it reflects it completely it appears white (Petela, 2010). Making judgments on the blackness of an object based entirely on the eye can be misleading considering that visible radiation occupies a narrow band of the spectrum. An example of this would be snow, which reflects light and hence appears white but strongly absorbs long-wavelength radiation and are essentially black for infrared radiation (Cengel, 2006). It is possible to make a surface approach blackbody behavior by coating it with lampblack paint (Levine, 2002).

The emissive power computed with the Stefan-Boltzmann law is the summation of the energy emitted by a blackbody over all wavelengths (Silbey et al., 2005). But sometimes one may be interested with the radiation emitted by a blackbody at an absolute temperature, per unit surface area, per unit time, and more importantly per unit wavelength (Duffie & Beckman, 2013). Such quantity is known as spectral body emissive power (Duffie & Beckman, 2013). In 1901 Max Planck developed the relation for the spectral body emissive power which came to be known as Planck's law (Welty et al., 2008). The relation is expressed as:

$$\mathrm{E}_{b\lambda}(\lambda, \mathrm{T}) = \frac{\mathrm{C}_1}{\lambda^5[\exp(C_2/\lambda T) - 1]} \qquad (2\text{-}7$$

Where:

$C_1 = 2\pi h c_0^2 = 3.742 \times 10^8 \ W.\mu m^4/m^2$

$C_2 = hc_0/k = 1.439 \times 10^4\ \mu m.K$

T = absolute temperature of the surface

k = 1.38065 × 10^{-23} is the Boltzmann's constant.

Planck's law applies to surfaces in a vacuum or a gas (Modest, 2014). When dealing with other mediums, it is necessary to replace C_1 by C_1/n^2, knowing that n is the index of refraction of the medium (Cengel, 2006). A very important detail to remember is that term spectral is an indication of the dependence on the wavelength. Plotted in Figure 2-3 is the variation of spectral blackbody emissive power with wavelength at different temperature. A number of observations can be made from this figure.

- First, the radiation emitted at any specified temperature increases with wavelength up to a peak then starts to decrease with increase in wavelength. This means the emitted radiation is continuous function of wavelength (Cengel, 2006).
- Second, the amount of radiation emitted increases with increasing temperature and that regardless of wavelength (Cengel, 2006).
- Third, temperature increase causes a shift of the curves to the left toward the shorter-wavelength region. Thus the largest amount of radiation are emitted at shorter wavelengths and higher temperature (Cengel, 2006).
- Last but not least, the radiation emitted by the sun reaches its highest point in the visible region of the spectrum and thus the sun is tuned with our eyes. The curve also show that surfaces at T ≤ 527 °C emit most of their radiation in the infrared region and consequently cannot be detected by the human eye unless they reflect light coming other sources (Cengel, 2006).

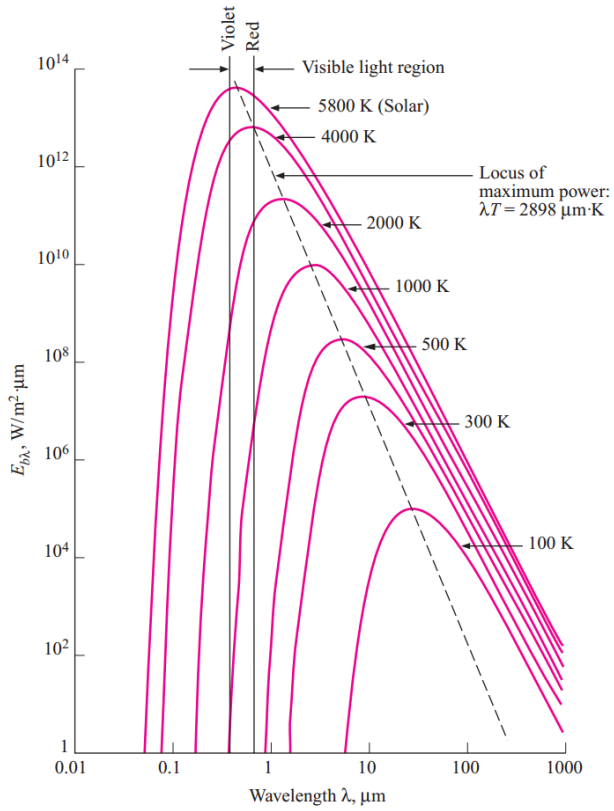

Figure 2-8: Spectral body emissivity as a function of wavelength for different values of T (Cengel, 2006)

In 1894 Willy Wien using classical thermodynamics developed an expression which gave the wavelength at which the highest peak in Figure 2- occur for a specified temperature (Petela, 2010). The correlation is known as Wien's displacement law and is expressed as:

$$(\lambda, \mathrm{T})_{\mathrm{max\,power}} = 2897.8\ \mu\mathrm{m.\,K} \qquad (2\text{-}8$$

Another way to obtain Wien's displacement law is to differentiate Planck's law with respect to the wavelength while holding the temperature constant and setting the results equal to zero (Silbey et al., 2005). The locus of maximum power which is a plot of Wien's law is also represented in Figure **2-**

One should notice that integrating Planck's law over all wavelengths gives the Stefan-Boltzmann law (Matzler, 2006). In mathematical terms:

$$\mathrm{E}_b(\mathrm{T}) = \int_0^\infty E_{b\lambda}\,(\lambda, \mathrm{T})\,\mathrm{d}\lambda = \sigma T^4 \qquad (2\text{-}9)$$

Basically the integral of the spectral blackbody emissive power over the entire wavelength spectrum is the total blackbody emissive power (Cengel, 2006).

1.8 Radiative properties

1.8.1 Emissivity

The emissivity of a surface, denoted by ε, measures how closely that surface resembles a blackbody (Kuehn, Ramsey, & Threlkeld, 1998). It is a ratio of the radiation emitted by a surface at a given temperature to that emitted by a blackbody at the same temperature (Hollands, 2004). Since no surface can emit more than a blackbody at a given temperature, the emissivity of a surface varies between zero and one (Brown et al., 2012). The emissivity of real surfaces unlike that of a blackbody is not constant. It is a function of the temperature of the surface as well as the direction wavelength and the direction of the emitted radiation (Silbey et al., 2005). Hence, depending on the effects considered one can define different emissivity for a given surface. Emissivity can also be defined in terms of spectral quantities. The smallest emissivity of a surface at any given temperature is the spectral directional emissivity, representing the ratio of radiation emitted by the surface at a specific wavelength in a specified direction to the intensity of radiation emitted by a blackbody under the same conditions (Cengel, 2006). In mathematical terms:

$$\varepsilon_{\lambda,\theta}(\lambda,\theta,\phi,\mathrm{T}) = \frac{I_{\lambda,\mathrm{e}}(\lambda,\theta,\phi,\mathrm{T})}{I_{\lambda,\mathrm{b}}(\lambda,\mathrm{T})} \qquad (2\text{-}10)$$

The subscripts:

- λ and θ are an indication of the spectral and directional nature of quantity of interest, respectively.
- e and b indicate the emissivity of the real surface and that of a blackbody respectively.

In equation (2-10) θ is the zenith angle and φ is azimuth used in the spherical coordinates system (Holman, 2010). The radiation emitted by a blackbody are independent of direction and thus the quantity in the denominator of equation (2(2-10) has no functional dependence on θ and φ (Incropera et al., 2007). The quantity I_e (θ, φ) in equation (2-10) is the spectral radiation intensity which is the rate of emission of radiant energy "$\dot{Q}_e$" in the (θ, φ) direction per unit area perpendicular to this direction and per unit solid angle about this direction (Cengel, 2006).

$$I_{\mathrm{e}}(\theta,\phi) = \frac{d\dot{Q}_e}{dA\cos\theta\cdot d\omega} = \frac{d\dot{Q}_e}{dA\cos\theta\sin\theta\, d\theta \mathrm{d}\phi} \qquad (2\text{-}11)$$

For a blackbody at an absolute temperature T and wavelength λ the spectral intensity of radiation is given by

$$I_{\lambda,\mathrm{b}}(\lambda,\mathrm{T}) = \frac{2hc_0^2}{\lambda^5[\exp(hc_0/\lambda\mathrm{kT})-1]} \qquad (2\text{-}12)$$

The spectral nature of equation (2-10) can be eliminated by integrating the spectral intensities over all wavelengths (Duffie & Beckman, 2013). Thus the spectral directional emissivity can be defined as

$$\varepsilon_{\theta}(\theta, \phi, \mathrm{T}) = \frac{I_{\mathrm{e}}(\theta, \phi, \mathrm{T})}{I_{\mathrm{b}}(\mathrm{T})} \tag{2-13}$$

Many practical applications have shown that it is sometimes more convenient to average radiation properties over all directions (Welty et al., 2008). Properties averaged in such manner are called hemispherical properties (Welty et al., 2008). Following that logic, the spectral hemispherical emissivity given by equation (2-14) can be defined as the integral of the spectral directional emissivity over all the directions in the hemisphere (Nellis & Klein, 2009). In mathematical terms

$$\varepsilon_{\lambda}(\lambda, \mathrm{T}) = \int_{\phi=0}^{2\pi} \int_{\theta=0}^{\pi/2} \varepsilon_{\lambda,\theta}(\lambda, \theta, \phi, \mathrm{T}) = \frac{E_{\lambda}(\lambda, \mathrm{T})}{E_{\mathrm{b}\lambda}(\lambda, \mathrm{T})} \tag{2-14}$$

And finally, integrating equation (2-14) over all wavelengths yield:

$$\varepsilon(\mathrm{T}) = \frac{E(\mathrm{T})}{E_{\mathrm{b}}(\mathrm{T})} \tag{2-15}$$

Equation ((2-15) shows for any given surface at a specific temperature, the total hemispherical emissivity is given by the ration of the total radiation energy emitted by the surface to that emitted by a blackbody having the same surface area and temperature.

Using equation (2-14) the following relation can be derived:

$$E_{\lambda}(\lambda, \mathrm{T}) = \varepsilon_{\lambda}(\lambda, \mathrm{T}) E_{\mathrm{b}\lambda}(\lambda, \mathrm{T}) \tag{2-16}$$

And according to the definition of spectral quantities:

$$E(\mathrm{T}) = \int_{0}^{\infty} E_{\lambda}(\lambda, \mathrm{T})\, d\lambda \tag{2-17}$$

Substitution of equation (2-16) in (2-17) yield:

$$E(\mathrm{T}) = \int_{0}^{\infty} \varepsilon_{\lambda}(\lambda, \mathrm{T}) E_{\mathrm{b}\lambda}(\lambda, \mathrm{T})\, d\lambda \tag{2-18}$$

And finally the substitution of equation (2-18) and Planck's law in equation (2-15) yield:

$$\varepsilon(\mathrm{T}) = \frac{E(\mathrm{T})}{E_{\mathrm{b}}(\mathrm{T})} = \frac{\int_{0}^{\infty} \varepsilon_{\lambda}(\lambda, \mathrm{T}) E_{\mathrm{b}\lambda}(\lambda, \mathrm{T})\, d\lambda}{\sigma T^4} \tag{2-19}$$

The evaluation of this integral requires the knowledge of how the spectral emissivity varies with wavelength at the specified temperature. The integral in equation (2-19**)** is complicated enough that most of the times requires the use of numerical integration (Cengel, 2006). Still, it

is possible to simplify the integration by writing the emissivity as a step function i.e. diving the range into a number of wavelength bands and assuming the emissivity to be constant within those bands (Bird et al., 2002). The simplification sacrifices a little bit of accuracy while making the integral more convenient (Cengel, 2006). Take Figure for instance, the actual variation of emissivity plotted there can be approximated as:

$$\varepsilon_\lambda = \begin{cases} \varepsilon_1 = constant, & 0 \le \lambda < \lambda_1 \\ \varepsilon_2 = constant, & \lambda_1 \le \lambda < \lambda_2 \\ \varepsilon_3 = constant, & \lambda_2 \le \lambda < \infty \end{cases}$$

Then the integral function in equation (2-19) can be rewritten as:

$$\varepsilon(\mathrm{T}) = \frac{\varepsilon_1 \int_0^{\lambda_1} E_{\mathrm{b}\lambda}\, d\lambda}{E_{\mathrm{b}}} + \frac{\varepsilon_2 \int_{\lambda_1}^{\lambda_2} E_{\mathrm{b}\lambda}\, d\lambda}{E_{\mathrm{b}}} + \frac{\varepsilon_3 \int_{\lambda_2}^{\infty} E_{\mathrm{b}\lambda}\, d\lambda}{E_{\mathrm{b}}} \qquad (2\text{-}20)$$
$$= \varepsilon_1 f_{0-\lambda_1}(T) + \varepsilon_2 f_{\lambda_1-\lambda_2}(T) + \varepsilon_3 f_{\lambda_2-\infty}(T)$$

The general form of equation (2-20) is:

$$\varepsilon = \sum_{j=1}^{n} \varepsilon_j \Delta f_j$$

Where Δf_i represents an energy increment in the blackbody spectrum and can be determined from the tables compiled by Sargent found in various reference books (Bird et al., 2002).

When the energy increments $\Delta f i$ are equal, equation (2-22) takes the form (Duffie & Beckman, 2013):

$$\varepsilon = \frac{1}{n} \sum_{j=1}^{n} \varepsilon_j$$

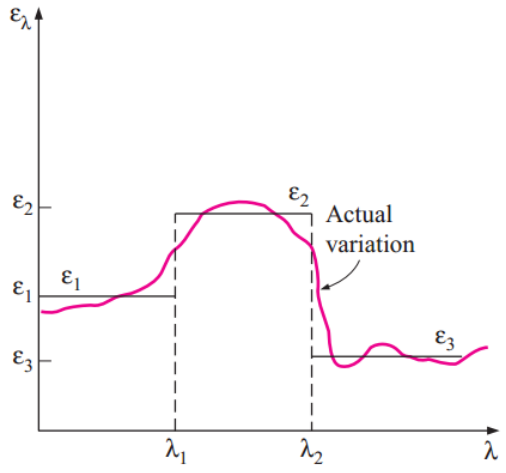

Figure2-9: Segmentation of emission spectrum into n parts (Cengel, 2006)

Radiation is a complex enough subjects and the fact that its properties depend on wavelength and direction does not help at all. Thus to simplify calculations some approximation are often employed (Bird et al., 2002). First there is diffuse surface approximation stating that the emissivity of this surface is constant (Bird et al., 2002). Diffuse surfaces are known to have properties that are independent of direction (Bergman et al., 2011).

Second there is the gray surface approximation which like the previous one states that the emissivity of a gray surface is constant (Duffie & Beckman, 2013). Gray surfaces have properties which are independent of wavelength (Kotz et al., 2012). Thus if a surface is both diffuse and gray then its emissivity will be equal to the total hemispherical emissivity at the surface temperature.

1.8.2 Absorptivity, reflectivity, and transmissivity

All forms of matter constantly emits radiation but this also implies that they are constantly bombarded by radiation from every direction emitted or reflected by other surfaces (Geankoplis, 1993). Upon contact with a surface some of the incident radiation are absorbed, some is reflected and the remaining is transmitted (Nellis & Klein, 2009). These fraction are called: absorptivity "α" when absorbed by the surface, reflectivity "ρ" when reflected by the surface and transmissivity "τ" when transmitted by the surface (Modest, 2014). Now let G be the irradiation defined as radiation flux incident on a surface from all directions (Modest, 2014). It can be expressed in mathematical terms as

$$G = \int_{hemisphere} dG = \int_{\phi=0}^{2\pi} \int_{\theta=0}^{\pi/2} I_i(\theta, \phi) \cos\theta \sin\theta \, d\theta d\phi \qquad (2\text{-}21)$$

The subscript "i" in equation (2-21) shows that the radiation intensity is incident.

Using the definition of G, the following quantities can be defined:

$$Absorptivity: \quad \alpha = \frac{Absorbed\ radiation}{Incident\ radiation} = \frac{G_{abs}}{G} \qquad (2\text{-}22$$

$$Reflectivity: \quad \rho = \frac{Reflected\ radiation}{Incident\ radiation} = \frac{G_{ref}}{G}$$

$$Transmissitivity: \quad \tau = \frac{Transmitted\ radiation}{Incident\ radiation} = \frac{G_{tr}}{G} \qquad (2\text{-}23$$

Where the subscripts abs, ref, and tr represent the absorbed, reflected and transmitted portions of the total incident radiation energy respectively. The first law of thermodynamics requires the following mathematical statement to be true (Petela, 2010):

$$G_{abs} + G_{ref} + G_{tr} = G \qquad (2\text{-}24)$$

Division of the terms in equation (2-24) by G yields

$$\alpha + \rho + \tau = 1 \tag{2-25}$$

Opaque surfaces do not transmit light meaning for them τ = 0 (Hollands, 2004), hence

$$\alpha + \rho = 1 \tag{2-26}$$

Equation (2-26) is a very important relation for opaque surfaces since it makes it possible to determine both the absorptivity and reflectivity from the knowledge of either of these properties.

Keeping in mind that G is the radiation flux coming on a surface over the hemispherical space and over all wavelengths, the properties α, ρ, and τ represent the averages of a medium over all directions and wavelengths (Duffie & Beckman, 2013). In other word they are total hemispherical properties. However, like emissivity the spectral directional *absorptivity* and *reflectivity* can be defined as:

$$\alpha_{\lambda,\theta}(\lambda,\theta,\phi) = \frac{I_{\lambda,\mathrm{abs}}(\lambda,\theta,\phi)}{I_{\lambda,\mathrm{i}}(\lambda,\theta,\phi)}$$

$$\rho_{\lambda,\theta}(\lambda,\theta,\phi) = \frac{I_{\lambda,\mathrm{ref}}(\lambda,\theta,\phi)}{I_{\lambda,\mathrm{i}}(\lambda,\theta,\phi)}$$

And the spectral hemispherical absorptivity, reflectivity, and transmitivity can be defined as:

$$\alpha_{\lambda}(\lambda) = \frac{G_{\lambda,\mathrm{abs}}(\lambda)}{G_{\lambda}(\lambda)}$$

$$\rho_{\lambda}(\lambda) = \frac{G_{\lambda,\mathrm{ref}}(\lambda)}{G_{\lambda}(\lambda)}$$

$$\tau_{\lambda}(\lambda) = \frac{G_{\lambda,\mathrm{tr}}(\lambda)}{G_{\lambda}(\lambda)}$$

Unlike the other radiative properties reflectivity has a bidirectional nature i.e. for any given surface the value of the reflectivity depends on both the direction of incident radiation and the direction of reflection (Hottel et al., 2008). The different types of reflective beams from radiation incident on a real surface are shown in Figure 2-7. The irregular shape is the type of reflection encountered in real life when a radiation beam is reflected on real surface (Howell, Menguc, & Siegel, 2016). Unfortunately detailed reflectivity data pertaining to irregular shaped reflection are not available for most surfaces (Cengel, 2006). Thus, during radiation calculations surfaces are assumed to reflect incident radiation in specular or diffuse manner (Cengel, 2006). During specular reflection, the angle of incidence and that of reflection are equals (Howell et al., 2016). Whilst in diffuse reflection, the incident beams are reflected equally in all the directions (Howell et al., 2016).

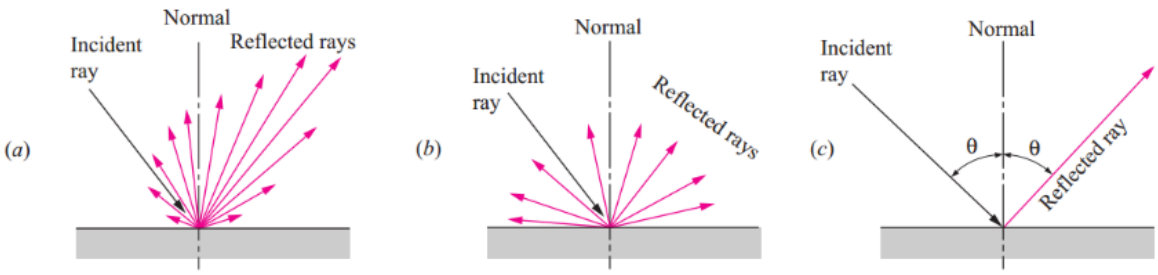

Figure 2-7: different forms of surface reflection: (a) actual or irregular, (b) diffuse, and (c) specular or mirror-like (Cengel, 2006)

There are two types of surfaces identified in reflection analyses: smooth and rough surfaces (Brewster, 1992). The former approximate specular reflection while the later are more close to diffuse reflection (Kuehn et al., 1998). The smoothness of a surface is defined in terms of height of surface roughness and wavelength of incident radiation (Kuehn et al., 1998). For a surface to qualify as smooth, the height of the surface roughness must be very small when compared to the wavelength of the incident radiation (Howell et al., 2016).

The absorptivity of a material has been known to be virtually independent of the surface temperature (Geankoplis, 1993). Rather it strongly influenced by the temperature of the source emitting the incident radiation (Bergman et al., 2011). An illustration of this fact is given in Figure2-8 where one can see that the absorptivity of concrete is 0.6 for a source temperature of 5780 K (Sun) and 0.9 for a source temperature of 300 K emanating from trees and buildings (Cengel, 2006).

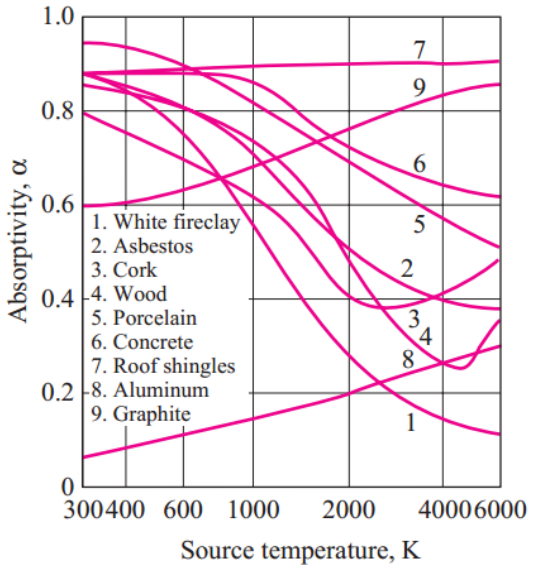

Figure2-8: Variation of absorptivity with

Another interesting trend is displayed on Figure2-8, that is: the absorptivity of metals increases with the source temperature while the opposite is true for electric nonconductors (Cengel, 2006). The more the surface appears white to the eye, the more pronounced the decrease in absorptivity with the source temperature will be (Welty et al., 2008).

The relation between emissivity and absorptivity of a surface is given by Kirchhoff's law which reads: "the total hemispherical emissivity of a surface at temperature T is equal to its total hemispherical absorptivity for radiation coming from a blackbody at the same temperature (Cengel, 2006)." in mathematical terms:

$$\varepsilon(\mathrm{T}) = \alpha(\mathrm{T}) \tag{2-27}$$

The spectral form of Kirchhoff law is:

$$\varepsilon_\lambda(\mathrm{T}) = \alpha_\lambda(\mathrm{T}) \tag{2-28}$$

Kirchhoff's law was derived for conditions where the surface and radiation source had equal temperatures (Levine, 2002). Thus it can only be used accurately for cases where the temperature difference between the surface and source temperature is less than a few hundred degrees (Levine, 2002).

Using Kirchhoff's law, equation (2-2) and (2-3) can be rewritten in terms of reflectance as (Duffie & Beckman, 2013):

$$\varepsilon = 1 - \sum_{j=1}^{n} \rho_j \Delta f_j$$

$$\varepsilon = 1 - \frac{1}{n}\sum_{j=1}^{n} \rho_j$$

Applying a similar reasoning to the one used for emissivity with the only difference being that the incident radiation must be specified, equation (2(2-15) through (2-3) can be derived in terms the absorptance to give:

$$\alpha = \sum_{j=1}^{n} \alpha_j \Delta f_j = \sum_{j=1}^{n} (1 - \rho_j)\Delta f_j = 1 - \sum_{j=1}^{n} \rho_j \Delta f_j$$

When the energy increments Δ*f*i are equal, equation (2-10) takes the form:

$$\alpha = \frac{1}{n}\sum_{j=1}^{n} \alpha_j = \frac{1}{n}\sum_{j=1}^{n} (1 - \rho_j) = 1 - \frac{1}{n}\sum_{j=1}^{n} \rho_j \tag{2-11}$$

1.9 Selective surfaces

Solar collectors are selective surfaces designed to have a high solar absorptance and low-wave emittance (Duffie & Beckman, 2013). The collectors are supposed to behave as a

blackbody absorbing as much incoming solar radiation as possible while at the same time minimizing energy losses by infrared radiation (Shimizu et al., 2014). In fact, most of the solar radiation (98 %) have a wavelengths less than 3.0 μm thus in order to be considered cost effective, any commercially available solar collector must be able to absorb at least 95 % of the incoming radiation and emit less than 0.05 % (Shimizu et al., 2014).

That goal can be achieved by designing an idealized selective surface with a very low reflectance below the cutoff wavelength (λ_C = 3.0 μm for instance) (Duffie & Beckman, 2013). Since for opaque surfaces $\alpha_\lambda = 1 - \rho_\lambda$, the surface will have a very high absorptance in this range. Then for wavelengths greater than λ_C the reflectance will be close to unity, and keeping in mind that $\varepsilon_\lambda = \alpha_\lambda = 1 - \rho_\lambda$, the surface's emittance will be very low in this range (Duffie & Beckman, 2013). An example of this concept is illustrated in Figure.

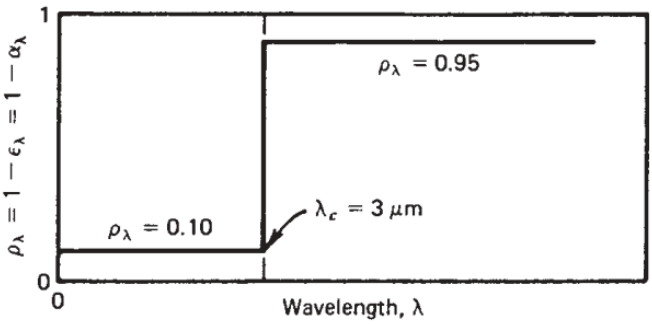

Figure2-17: hypothetical selective surface with a cutoff wavelength equal to 3 μm (Duffie & Beckman, 2013)

The different types of selective absorbing surfaces commercially available are: intrinsic absorbers, absorber-reflector tandems, multilayered interference stacks, optical trapping systems, selective paints, composite materials films and quantum-size effect materials (Shimizu et al., 2014).

1.9.1 Transparent conducting oxide (TCO) as solar absorber

Early on in this report the concept of CSP was introduced showing its great potential for large scale power generation using solar energy. The basic components of a typical CSP system would be: a solar receiver, reflectors, a thermal storage tank, a steam turbine and an electricity generator. CSPs used in modern day applications are usually operated around 550 ºC (Shimizu et al., 2014). But since those applications make use of the steam-turbine Rankin cycle, it is possible to greatly improve the efficiency of the system by increasing the system temperature to more than 800 ºC (Stadler, 2012). The problem is that commercially available thermal absorbers cannot be utilized at temperatures greater than 500 ºC (Nuru, 2014). In fact, as dictated by Wien's displacement law, the highest peak of thermal radiation shifts

toward shorter wavelength region as the temperature increases. Thus these absorbers tend to lose a significant amount of radiation in the near infrared range at high temperatures (Ginley, Bright, & Editors, 2000).

One of the approaches that can be used to restore the spectral selective property of the absorber (substrate) is to coat it with transparent conducting oxide or TCO (Shimizu et al., 2014). In fact, the studies conducted by Haitjema and Elich (1987), Fan and Bachner (1976), Shimizu et al. (2014), and Nuru (2014) showed that applying a coating of TCO on substrates such as window glass, Pyrex, black enameled steel, tantalum, and cupper, increased the solar absorbance of the substrate for temperatures as high as 700 ºC.

TCOs are materials characterized by a good electrical conductivity, relatively low absorption of radiation in the visible spectrum, and high reflectance for radiation in the IR spectrum (Stadler, 2012). Basically they are electrical conductor, transparent to light, and opaque for IR radiation.

TCOs are generally composed of two parts: metallic A and nonmetallic B (Stadler, 2012). the metallic part usually consists of a single or combinations of metals while the nonmetallic part is always oxygen (Stadler, 2012). The type of metals used give rise to various opto-electrical characteristics which can be modified by doping the TCO with a metal, metalloid or nonmetals (Edwards, Porch, Jones, Morgan, & Perks, 2004). Thus it is possible to have a system where an element is used both in the metallic part A and as dopant D (Stadler, 2012).

1.9.2 Correlations of optical and electrical properties for TCOs

Optical phenomenon within the infrared region are given by Drude's theory of free electrons in metals (Nuru, 2014). Free electrons interact with an electromagnetic field leading to a polarization of the field within the material and consequently changing the relative permittivity ϵ (Lewis & Paine, 2000a). The relative permittivity according to Drude's theory is given by:

$$\epsilon = (n - ik)^2 \tag{2-30}$$

$$\epsilon^{'} = n^2 - k^2 = \epsilon_\infty \left(1 - \frac{\omega_p^2}{\omega^2 + \gamma^2}\right) \tag{2-31}$$

Also,

$$\epsilon^{"} = 2nk = \frac{\omega_p^2 \gamma \epsilon_\infty}{\omega(\omega^2 + \gamma^2)} \tag{2-32}$$

Where:

- ω is the optical frequency;

- ω_p is the plasma resonance frequency as is defined as

$$\omega_p = (4\pi N e^2/\epsilon_0 \epsilon_\infty m_e^*)^{1/2} \quad (2\text{-}33)$$

- The parameters ϵ_∞ and ϵ_0 are the dielectric constants characteristic of the medium and free space, respectively;
- m_e^* is the effective mass of the charge carriers (conduction band electrons);
- N represents the concentration of conduction band electrons;
- e is the electronic charge;
- γ is the frequency of collision given by:

$$\gamma = \frac{1}{\tau_e} = -\frac{e}{m_e^* \mu} \quad (2\text{-}34)$$

Where τ_e is the relaxation time and μ the electron mobility

The parameters n and k are optical constants that dictates the magnitude of the reflectance and absorbance of a surface (Edwards et al., 2004). Drude's theory makes it possible to relate the optical constants n and k to the electron's density N and mobility μ which are electrical constants (Edwards et al., 2004).

Drude's theory relies on the assumption that the relaxation time is independent of frequency (Ginley et al., 2000). The theory takes different forms depending on whether the frequency is in the absorbing, reflecting or transmitting region.

Case 1: absorbing region $0 < \omega\tau_e < 1$

This region is characterized by a strong reflectance of transparent conducting films caused by the large difference in magnitude of between the imaginary ϵ' and real ϵ" parts of Drude's theory. Within this region $\epsilon" \gg \epsilon'$ and equations (2-31) and (2-32) become:

$$\epsilon' = \epsilon_\infty\left(1 - \omega_p^2 {\tau_e}^2\right)$$

$$\epsilon" = \epsilon_\infty \frac{\omega_p^2 \tau_e}{\omega} \gg 1$$

From (2-12) and (2-13) equations, the Hagen-Ruben relation can be defined:

$$n^2 = k^2 \frac{\epsilon_\infty \omega_p^2 \tau_e}{2\omega} \quad (2\text{-}35)$$

For instances where the skin depth $\delta\ (= \lambda/4\pi k)$ is much smaller than the layer thickness, the reflectivity of the layer is given by:

$$R = \frac{(n-1)^2 + k^2}{(n+1)^2 + k^2} \quad (2\text{-}36)$$

Substitution of equation (2-35) in (2-36) yield:

$$R = 1 - 2\left(\frac{2\omega}{\epsilon_\infty \omega_p^2 \tau_e}\right)^{1/2} \quad (2\text{-}37)$$

Case 2: reflecting region $1/\tau_e < \omega < \omega_p$

This region is also known as the relaxation region characterized by rapid decrease in absorption coefficient and $\omega^2\tau_e^2 > 1$. There is almost complete reflection within this region and the real part of the permittivity given by equation (2-31) is negative. The real and imaginary part (equations (2-31) and (2-32)) in this region are given by:

$$\epsilon' = \epsilon_\infty \left[1 - \left(\frac{\omega_p}{\omega}\right)^2\right] < 0$$

$$\epsilon'' = \epsilon_\infty \frac{\omega_p^2}{\omega^3 \tau_e} > 1$$

and the parameters n and k take the form:

$$n = \frac{\omega_p \epsilon_\infty^{1/2}}{2\omega^2 \tau_e}$$

$$k = \sqrt{\left(\frac{\omega_p}{\omega}\right)^2 - 1} \simeq \frac{\omega_p}{\omega} \epsilon_\infty^{1/2}$$

For instances where the skin depth δ is much smaller than the layer thickness, the reflectivity of the layer is given by:

$$R = 1 - \frac{2}{\omega_p \tau_e \epsilon_\infty^{1/2}} \quad (2\text{-}38)$$

Case 3: transparent region $\omega > \omega_p$

This region is characterized by a minimization of the reflective power and the parameter ϵ' taking on a positive value, making the films transparent. Within this region ϵ' and ϵ" are given by:

$$\epsilon' = \epsilon_\infty \left(1 - \left(\frac{\omega_p}{\omega}\right)^2\right) \quad (2\text{-}17)$$

$$\epsilon'' = \epsilon_\infty \frac{\omega_p^2}{\omega^3 \tau_e} \ll 1$$

and consequently, the parameters n and k take the form:

$$n \simeq \epsilon_\infty^{1/2} \sqrt{1 - \left(\frac{\omega_p}{\omega}\right)^2} \simeq \epsilon_\infty^{1/2} \quad (2\text{-}40)$$

$$k \simeq \epsilon_\infty^{1/2} \frac{\omega_p^2}{2\omega^3 \tau_e} \simeq 0 \quad (2\text{-}41)$$

A plot of the variation of n and k with wavelength for a given transparent semiconductor film is given in Figure2-. It shows that when $\lambda < \lambda_{pl}$ (where λ_{pl} is the plasma resonance wavelength) the value of n stays approximately constant at $\epsilon_{\infty}^{1/2}$. When λ nears λ_{pl} the reflectance decreases greatly and the value of n gets close to one. And when $\lambda > \lambda_{pl}$, n and k increases swiftly which result in a high reflectivity.

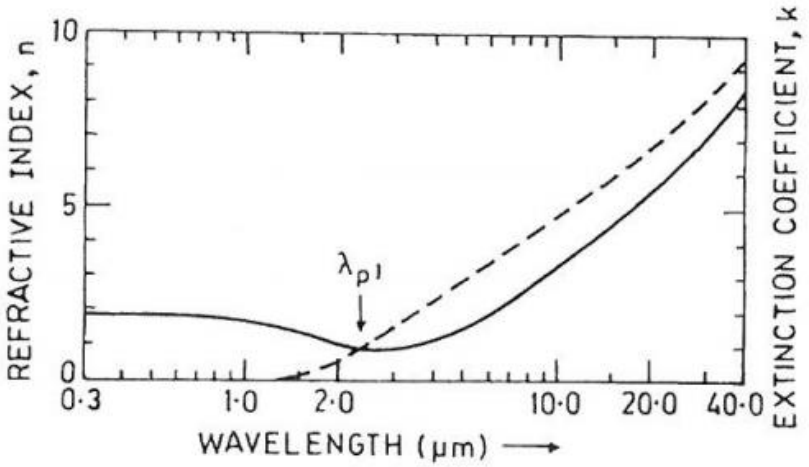

Figure2-13: Variation of n and k with wavelength for SnO_2 films: (—) n and (- - -) k

The carrier concentration plays two roles in the plot presented in Figure2-. First, it dictates the value of the value of the plasma wavelength in accordance with equation (2-33): the carrier concentration and the plasma wavelength are inversely proportional. Second, the maximum achievable reflectivity is a function of N. This is confirmed by plot shown in Figure2- where one can see that the reflectivity approaches unity for large values of N. The sample plotted in Figure2- 2-14 has a mobility of 15 cm^2/V s and $m^* = 0.25\ m_0$. The mobility has a similar effect on the infrared (IR) reflectivity of transparent conducting films with the difference being that change in the value of mobility does not directly influence the plasma wavelength.

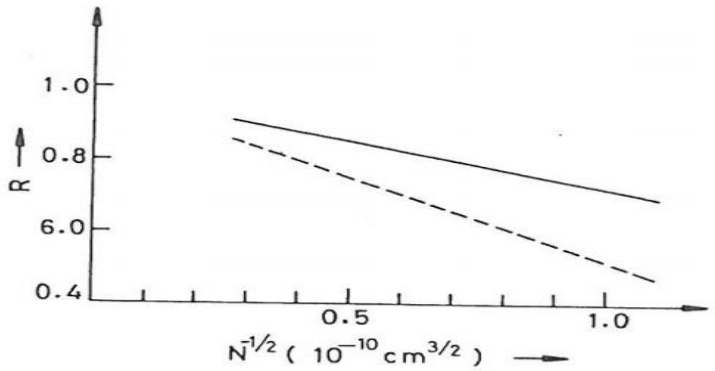

Figure2-14: IR reflectivity as a function of carrier concentration for two wavelengths: (—) 40 μm and (- - -) 10 μm

Various study have been conducted in order to test the validity of Drude's theory. The results of some these studies are presented in Figure2-2-15 Figure 2- and Figure. The general trend shows that experimental observations of transmittance and reflectance in fluorine-doped SnO_2 films and fluorinated indium tin oxide films fit with the predictions made by Drude's theory. Nevertheless, Figure2- shows that the theory somehow fails to explain the experimental results obtained near the plasma wavelength. The consensus is that Drude's theory makes accurate predictions only when restricted to a spectral region. This may stem from the fact that Drude's theory assumes the relaxation time to be constant over the entire spectral region while several studies report it to be frequency dependent.

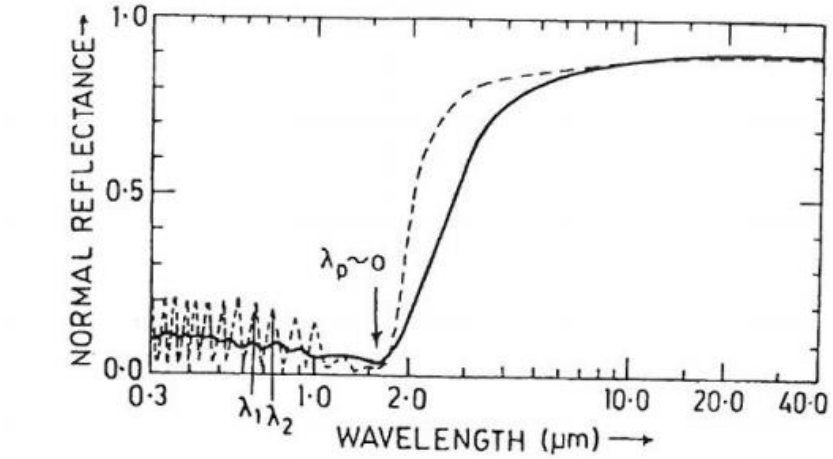

Figure2-15: Normal reflectance estimated using Drude's theory (- - -) and experiment (—) for fluorine-doped SnO2 where N = 3.5 x 10^{20} cm^{-3} and μ = 46 cm^2/V s

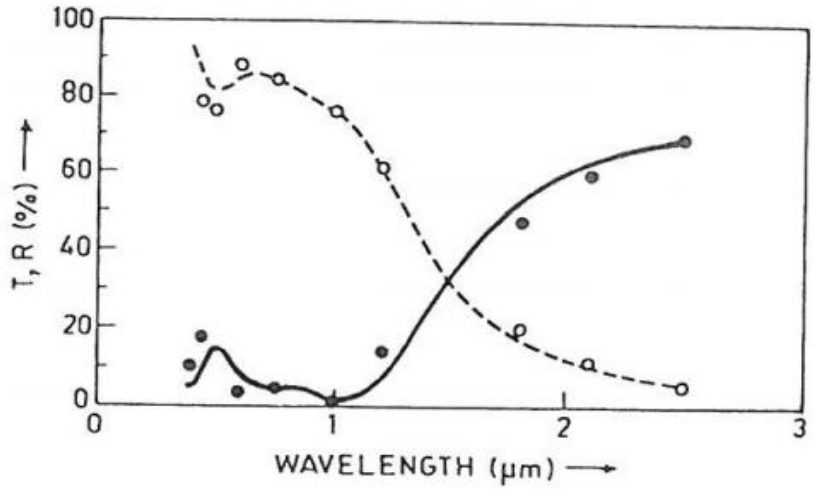

Figure 2-16: Optical transmittance and reflectance as a function of wavelength for fluorinated indium oxide films. Experimental (○, ●) and calculated (- - -) (—) respectively

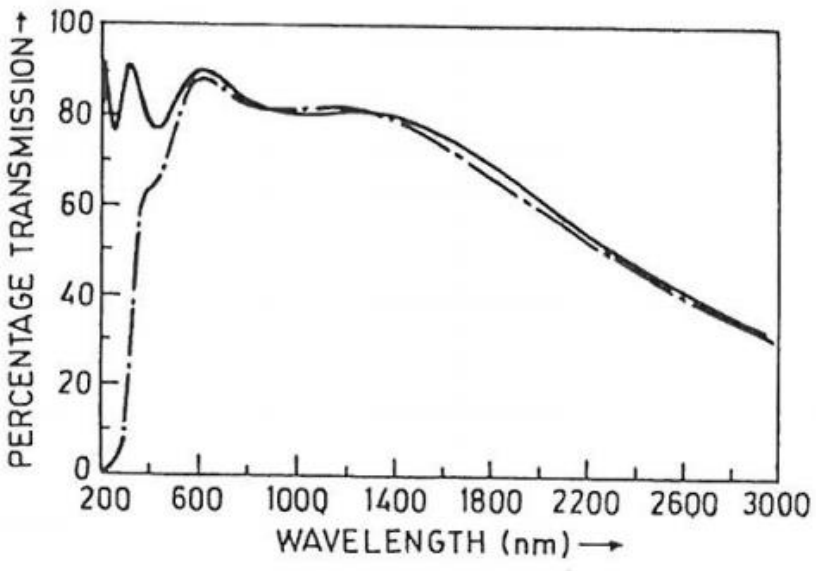

Figure2-17: optical transmittance in the visible and near-infrared for indium tin oxide films: Experimental (- - -) and Drude's fit (—).

Selective coatings for receivers can reduce losses and increase overall efficiency by maintaining a high absorptance in the solar spectrum but lowering emittance in the infrared spectrum. Such solar selective absorbers (SSAs) have been developed and deployed for more than three decades for lower temperature parabolic trough application (Kennedy, 2002).

However, these coatings are not well-suited for power tower applications; they are sensitive to oxidation and they can typically only operate at temperatures up to ~500°C before performance degrades.

Any novel selective absorber material developed for next-generation receivers must be stable in air, cost effective, and survive thousands of heating and cooling cycles (Kennedy & Price, 2005)(Patent, 2014). Many efforts have been sought to address the issue of highly efficient and durable SSAs for operating temperatures from 650°C to 1000°C (Olsen et al., 2014)(Nuru, 2013)(Yin & Collins, 1995). Among the different selective absorber materials developed to address the issue of thermal stability, are multilayered coatings of refractory metals, which have turned out to possess low emittance, high spectral selectivity, and good adhesion to the receiver surface (Gray, Tirawat, Kessinger, & Ndione, 2015). However, the oxidation resistances in air of these multilayered coatings have not been fully tested in a long term.

TCOs are an essential part of technologies that require both large-area electrical contact and optical access in the visible portion of the light spectrum.

High transparency, combined with useful electrical conductivity (> 10^3 $\Omega^{-1}cm^{-1}$), is achieved by selecting a wide bandgap oxide that is rendered degenerate through the introduction of native or substitutional dopants. Most of the useful oxide-based materials are *n*-type conductors that ideally have a wide bandgap (> 3 eV), the ability to be doped to degeneracy, and a conduction band shape (dictating an electron effective mass) that ensures that the plasma absorption edge lies in the infrared range (Lewis & Paine, 2000b).

The most widely used TCO in optoelectronic devices is tin-doped indium oxide (ITO). Other TCOs such as fluor-doped tin oxide (FTO) and aluminum-doped zinc oxide (AZO) are also available and find use in specialized applications where ease of deposition, cost, or IR reflectivity is favored over optimum optical transmission and minimum sheet resistance. For example, heat-efficient windows that reflect in the infrared range are created during the manufacture of architectural glass by means of the direct deposition of SnO_2 using chloride-based spray pyrolysis. In this passive application, good electrical conductivity is sacrificed for IR reflectivity, high transparency in the visible regime, and processing convenience and economics (Lewis & Paine, 2000b).

In a study reported by Shimizu et al (Shimizu et al., 2014) TCO was used as a solar selective absorber in power generation systems (CSP). Because TCO material has plasma wavelength in infrared region. Therefore, the electromagnetic waves with shorter wavelength than plasma wavelength go through the material, while the electromagnetic waves with longer wavelength are reflected on the surface. The study by Shimizu et al showed that TCO on metal substrate exhibited high performance as solar selective absorbers, i.e. high absorptance in visible light range and low emittance in infrared range by numerical simulations. The optical property of fabricated TCO coated metal is well consistent with the simulated property. High performance solar selective absorber of which solar absorptance is 0.71 and hemispherical total emittance is 0.11. The thermal stability is also confirmed at 600^{o}C in vacuum for 3hr (Shimizu et al., 2014).

TCO film has high spectral selectivity derived by plasma wavelength, though it has not gained popularity as a solar absorber previously. To confirm the viability of the solar selective absorber with TCO thin film, Shimizu et al. investigated TCO performance by means of a numerical simulation based on rigorous coupled-wave analysis (RCWA) method. Their simulation revealed that the absorptance is increased in short wavelength range by coating TCO on Ta substrate, though the absorptance remains low in long wavelength range. It was also realized that the absorptance in short wavelengths become increasingly pronounced as

the TCO thickness increases. The ITO coated Ta was prepared by RF-sputtering. The fabricated sample shows expected optical properties. The thermal stability at 600^{o}C was confirmed for only three hours by heating in vacuum. The figure of merit (FOM) calculated for the fabricated sample showed a value of 0.70. This value was not so high, but higher FOM would be obtained by controlling the cut-off wavelength of ITO to longer wavelength range by sn dopant concentration (Shimizu et al., 2014).

From their study, they verified the suitability of TCO for the solar selective absorbers which could be used at high-temperature and therefore contributes to improve energy efficiency of solar energy systems which is operated at high-temperature.

CHAPTER THREE

STRUCTURAL AND OPTICAL CHARACTERIZATION OF Al DOPED ZnO TRANSPARENT CONDUCTING OXIDE (TCO)

3.1 Introduction

This chapter provides a brief discussion of the synthesis of Al doped ZnO (AZO) thin films nanostructure using radio frequency RF magnetron sputtering process. The influence of the deposition parameters, including argon working pressure and substrate temperature, on the structural and optical properties of the AZO thin films is investigated by means of X-ray diffraction (XRD) and optical spectroscopy (UV-VIS-NIR). The optical constants of AZO films are extracted from transmittance and reflectance spectra using a combination of Drude and Lorentz dielectric function model as described in chapter two. The extracted optical constants will be used in the simulation of the solar spectral selectivity in the next chapter.

3.2 AZO thin films nanostructure synthesis

AZO thin films were deposited on glass substrates in a planar RF magnetron sputtering system Leybold Heraeus Z600 with a base pressure of 10^{-6} mbar. For thin film preparation a sintered ceramic target with a mixture of $ZnO:Al_2O_3$ (purity 99.995%) was used. The percentage of Al_2O_3 in the ZnO target was 2.5 wt%. To achieve a better structural homogeneity and thickness uniformity, the substrate holder was rotated at 15 rounds per minute during deposition. The glass substrates were cleaned chemically using acetone, trichloroethylene, and methanol for 5 minutes each in an ultrasonic bath. The substrates were then rinsed with distilled water and dried with dry nitrogen. They were then loaded in the vacuum chamber and subsequently RF plasma (Ar+10% O) cleaned for a period of 15 min to remove remaining organic contaminants and to improve film adhesion to substrate. Prior each deposition a pre-sputtering of 5 min was carried out to clean the target. The deposition time was maintained to 30 min .The argon gas pressure was ranged from 10^{-2} mbar to 10^{-3} mbar and the deposition temperature was set to 300 °C and room temperature. The deposition conditions are summarized in table 3.1.

The films structure (crystalline state, crystallite orientation and lattice strains) was investigated by an automatic powder X-ray diffractometer Philips X'Pert X'Pert PRO MPD. Copper Kα radiation (λ = 0.154 nm) was used. The optical transmittance and reflectance in ultra violet, visible and near infrared regions was determined by a spectrophotometer Cary 500.

Table 3.1: Deposition conditions of AZO thin films

RF Power	300 W
Sputtering gas	Argon
Working pressure	10^{-3} to 10^{-2} mbar
Target Diameter	127 mm
Substrate temperature	Ambient temperature and 300°C
Target–substrate distance	5 cm

3.3 Structural properties

Figure 3.1 shows the XRD patterns of AZO thin films nanostructure deposited at room temperature and 300 °C as well as at different Ar gas pressures. Regardless of the substrate temperature and the working gas pressure, All AZO films are polycrystalline with hexagonal structure and no metallic Zn or Al characteristic peaks are observed. At room temperature deposition, the crystallinity of the films decreases as reflected by (002) peak intensity when the Ar pressure is increased . For samples deposited at 300 °C and independently of the working pressure, XRD patterns show only (00.2) and (00.4) planes reflections confirming a strong preferred orientation of crystallites (texture) in [00.*l*] direction perpendicular to the substrate plane. For samples deposited at room temperature the [00.*l*] texture is significantly influenced by the Ar gas working pressure as shown in figure 3.1. For working pressure higher than $4x10^{-3}$ mbar the [00.*l*] texture deteriorates and the xrd spectra exhibit other reflections (10.0), (10.1) ,(11.0) and (10.3) beside the (00.2) reflection. The (00.4) reflection is absent for sample deposited at Ar pressure of 0.01 mbar. However at $4x10^{-3}$ mbar and lower pressures the [00.*l*] texture considerably improves and only (00.2) and (00.4) reflections are present and the texture at these conditions are very similar to the one exhibited by AZO film deposited at substrate temperature of 300 °C. This result shows that the texture is markedly influenced by the surface mobility of atoms during deposition. At lower pressure the sputtered atoms undergo less collision with Ar ions in the plasma and arrive at the substrate with enough energy that promotes surface diffusion. On the other hand at higher substrate temperature regardless of the working pressure, the adatoms acquire energy (~kT) from substrate to promote their surface diffusion.

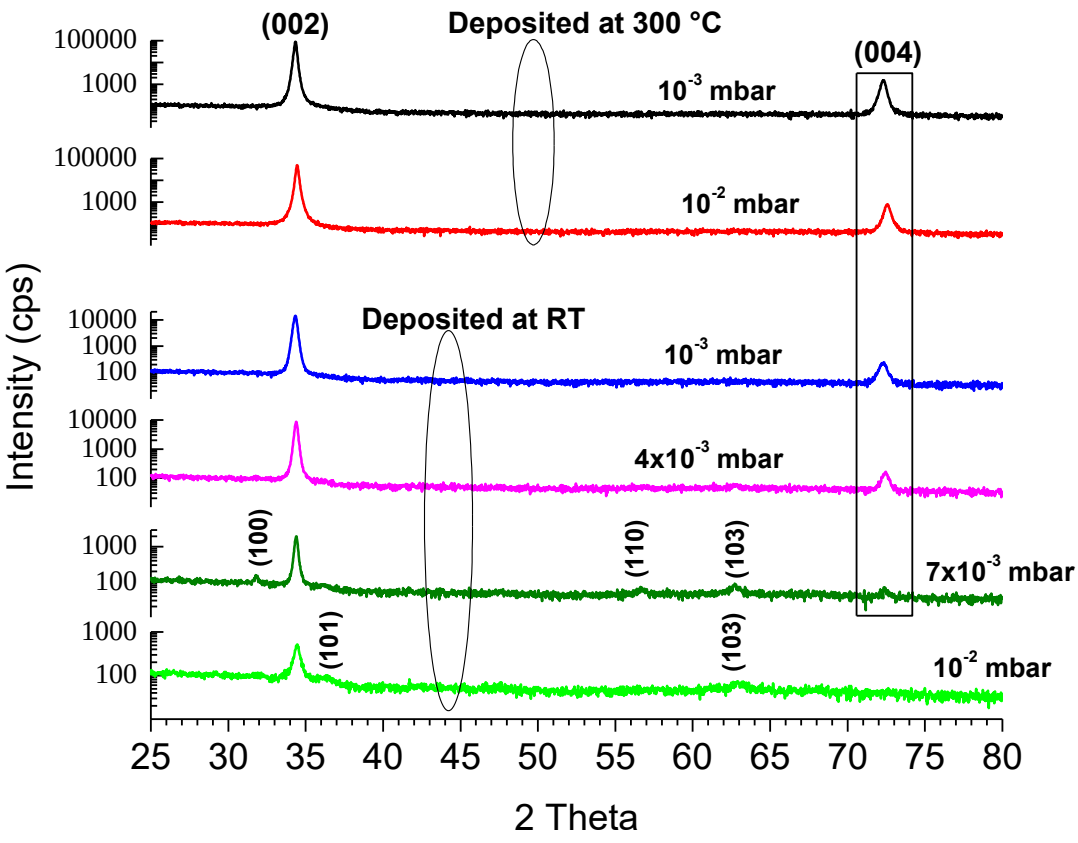

Figure 3-1: XRD patterns of AZO films deposited at RT and 300° C under different working gas pressures (Notice the Log scale of intensity)

Independently of the substrate temperature the XRD patterns shown in figures 3.2 and 3.3 reveal a peak shift towards the lower angles as the working pressure decreases indicating an intrinsic compressive stress (uniform strain) in the ZnO:Al films deposited at lower pressure (Cullity et al, 2014). Interestingly for the films deposited at the higher Ar gas pressure of 0.01 mbar the peak positions of the (00.2) and (00.4) reflections (34.44° and 72.56° respectively) are very close to the bulk ZnO peak positions given by JCPD file (34.42°and 72.56°). This confirms that these films are stress free. As depicted in figure 3.2 for samples deposited at 300°C, the peak shift occurs without a noticeable change in the peaks profile. The full widths at half maximum (FWHM) of (00.2) peaks for the film deposited at 10^{-3} and 10^{-2} mbar are basically the same (0.134°) and for (00.4) peaks the FWHMs are very close 0.201° and 0.192° respectively. Meanwhile for the films deposited at room temperature beside the peaks shift there is a significant broadening in the peak profiles as shown in figure 3.3. The FWHM increases with a decrease in Ar gas pressure. This broadening is more likely due to defects and development of micro-stress (non-uniform strain) in the films than a decrease in crystallite sizes since at lower pressure the adatoms have enough energy to promote crystallite growth

(Mattox et al, 2010). Therefore higher deposition temperature relieves micro-stress and "heals" defects as reflected by the absence of peaks profile broadening in the films deposited at 300°C.

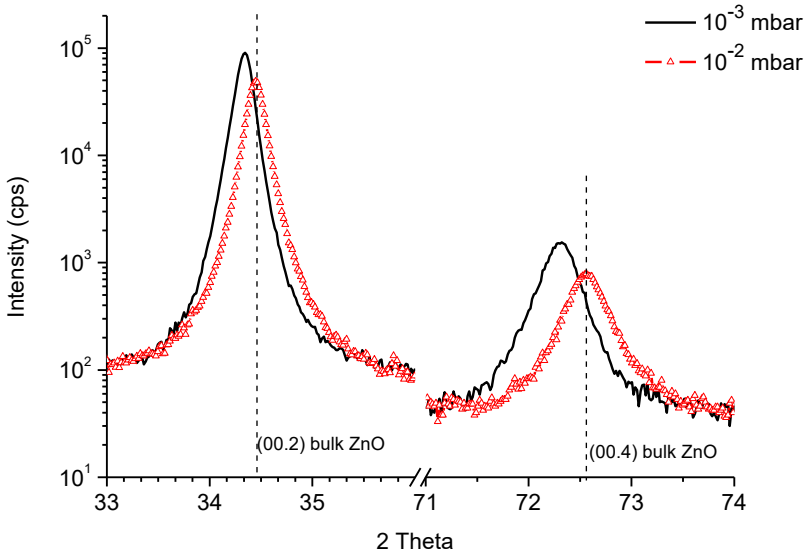

Figure 3.2: (00.2) and (00.4) peaks shift in AZO films deposited at 300° C under different working gas pressures (dashed line represent peaks position of bulk ZnO)

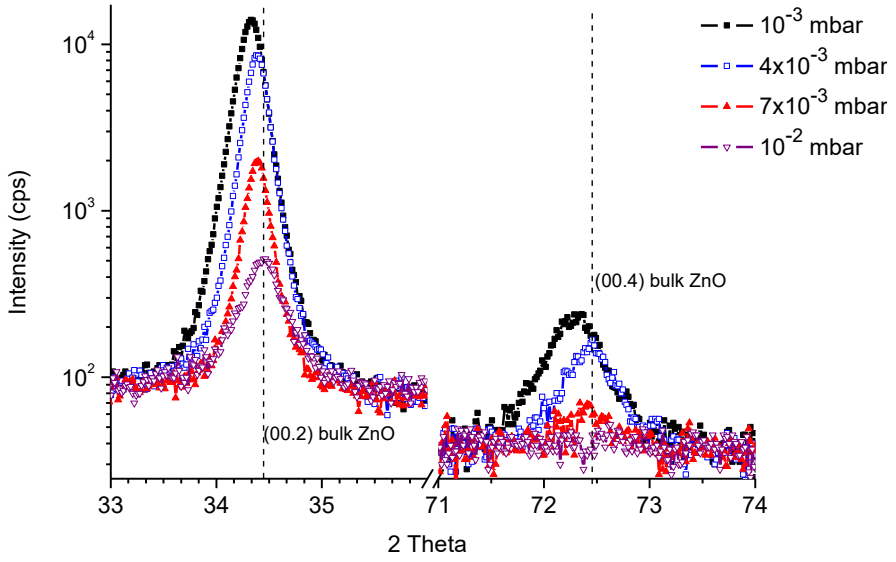

Figure 3.3: (00.2) and (00.4) peaks shift in AZO films deposited at RT under different working gas pressures (dashed line represent peaks position of bulk ZnO)

The uniform compressive stress present in the films is possibly caused by an atomic peening process by of recoil damage or forward sputtering (Windischmann, 1992)

The uniform compressive stress in the films can be estimated by calculating the strain in the films given by ε= (d-do)/do where d and do are the interplanar spacings of strained and unstrained crystal respectively. Considering the elastic modulus of ZnO:Al films is the same as the bulk ZnO, E=140 GPa (Jagadish et al, 2006) from Hooke's law the estimated compressive stress σ is given as σ=Eε. The strain and uniform compressive stress calculated from the (00.2) reflection are summarized in table 3.2

Table 3.2: Strain and uniform compressive stress in AZO films deposited at different temperature and Ar gas working pressure

Temperature	working pressure	d_{002} (nm)	ε (%)	σ (GPa)
300 °C	10^{-3} mbar	2.611	0.30	0.41
RT	10^{-3} mbar	2.612	0.31	0.44
RT	$4x10^{-3}$ mbar	2.608	0.18	0.25
RT	$7x10^{-3}$ mbar	2.607	0.14	0.20

From the results depicted in table 3.2 there is a clear evidence of the influence of deposition pressure on the development of uniform strain in the AZO films meanwhile the effect of the temperature is negligible as reflected by the close values of the strain and stress of the films deposited at same pressure (10^{-3} mbar) and different temperatures (RT and 300°C).

3.4 Optical properties

The optical transmittance of AZO films deposited at substrate temperature of 300 °C and working gas pressure ranging from 10^{-3} to 10^{-2} mbar is shown in figure 3.4. The Irrespective of working gas pressure the AZO films deposited at 300 °C displayed an average transmittance of about 85% in the 400–900 nm wavelength range and a sharp absorption edge at about 334 nm (estimated from the maximum derivative of transmittance in the range 300-400nm). This corresponds to an optical band gap value of 3.71 which is higher than the optical band gap of intrinsic ZnO (3.2 eV). The absorption edge towards the shorter wavelength is due to an increase in carrier concentration caused by Al doping and is mainly attributed to the Burstein–Moss effect, (Jagadish et al, 2006).

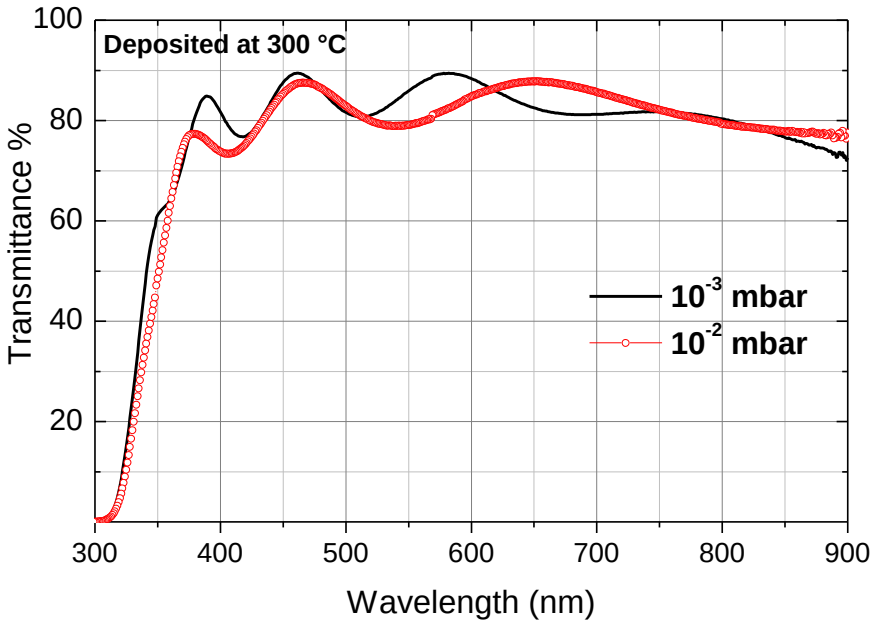

Figure 3.4: Transmittance spectra of AZO films deposited at 300 °C and under different working Ar gas pressures

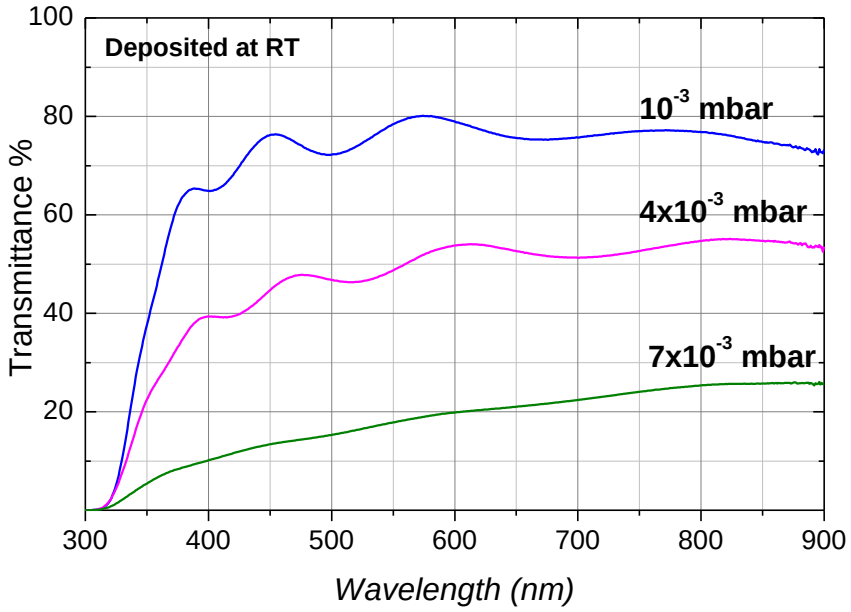

Figure 3.5: Transmittance spectra of AZO flms deposited at room temperature and under different working Ar gas pressures

Figure 3.5 shows the optical transmittance of AZO films deposited at RT under different working gas pressures. The transmittance of the films is strongly affected by the Ar pressure and it improves significantly at the lower pressure of 10^{-3} mbar. For this condition an average

transmittance of about 75% is recorded in the wavelength range of 400-900nm. This transparency is lower than the one obtained for films deposited at 300°C. This results reveal that the best optical properties of AZO is obtained for sputtering conditions where the substrate temperature is high and the deposition pressure is low. As shown in figure 3.6 AZO films deposited under this optimal synthesis conditions exhibit high transmittance in the visible and high reflectance in the infrared as required for a solar selective absorber.

To compute the solar absorptance and thermal emissivity for different configurations of AZO films we extracted the optical constant n and k in the wavelength range of 300-2500 nm from the transmittance and reflectance data of the well optimized AZO film deposited at 300°C under Ar pressure of 0.001mbar. To model the optical properties, Drude oscillator in combination of four Lorentzian oscillators of different resonant energies was necessary to describe the dispersion in the optical properties of the AZO thin film over the considered wavelength range as follows:

$$\varepsilon(\omega) = \varepsilon_{\infty} - \frac{\omega_p^2}{\omega(\omega + i.\gamma)} + \sum_j \frac{\omega p_j}{(\omega_{oj}^2 - \omega^2) - i.\gamma_{oj}.\omega} \qquad (3.1)$$

Where ε_∞ is the high-frequency dielectric constant, which represents the contribution of all oscillators at very high frequencies. The parameters ωp_j , ω_{oj} and γ_{oj} are the 'plasma' frequency, the transverse frequency (eigen-frequency) and the line-width (scattering rate) respectively of the j-th Lorentz oscillator. These are fitting parameters, together with the layer thickness, in the least-squares fit procedure, as implemented in Scout© software,which minimizes the biased estimator x2.
Reflectance and transmittance data have been fitted with a two-layer model including the bulk film, and the surface roughness. The latter was modelled as composite layer consisting of mixture of voids and AZO materials by using Bruggeman effective medium approximation (Edwards et al., 2004)

The best-fit result according to the two model substrate/film/roughness, is also shown in Figure 3.6 and the obtained fitting parameters are summarized in table 3.3

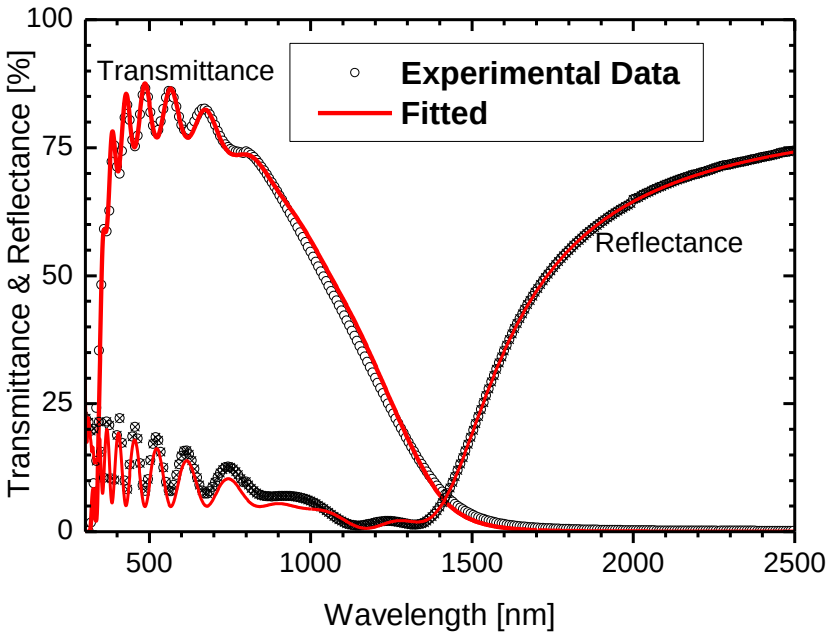

Figure 3.6: Experimental and simulated transmittance and reflectance of AZO film

Table 3.3: Optical parameters of AZO film calculated from reflectance and transmittance spectra.

AZO layer thickness : [nm]			674.6		
Composite AZO/voids layer thickness [nm]			58.2		
Voids volume fraction: [%]			23%		
high-frequency dielectric constant ε_∞ :[eV]			3.85		
Drude Oscillator:	Plasma frequency ωp [eV]		1.68		
	Damping Factor γ [eV]		0.23		
Lorentz Oscillators	Oscillator number	1	2	3	4
	ωp [eV]	2.204	1.671	0.281	1.576
	ωo [eV]	5.592	3.988	3.762	4.538
	γ [eV]	0.6356	0.0486	0.207	0.195

Figure 3.7 shows the dispersion of refractive index n and extinction coefficient k in the wavelength range 300-2500 nm derived from the Drude-Lorentz modelling of the experimental reflectance and transmittance data of AZO film. It is this data that was used in the transfer matrix model (Born et al, 1999) to simulate experimental transmittance and reflectance spectra. The reduction in refractive index n and the increase in the extinction coefficient k in the infrared spectrum is directly related to electric conductivity (i.e. free carrier absorption). It is this behaviour that gives higher reflectance in the infrared spectrum and which is of significance for thermal emittance for AZO films.

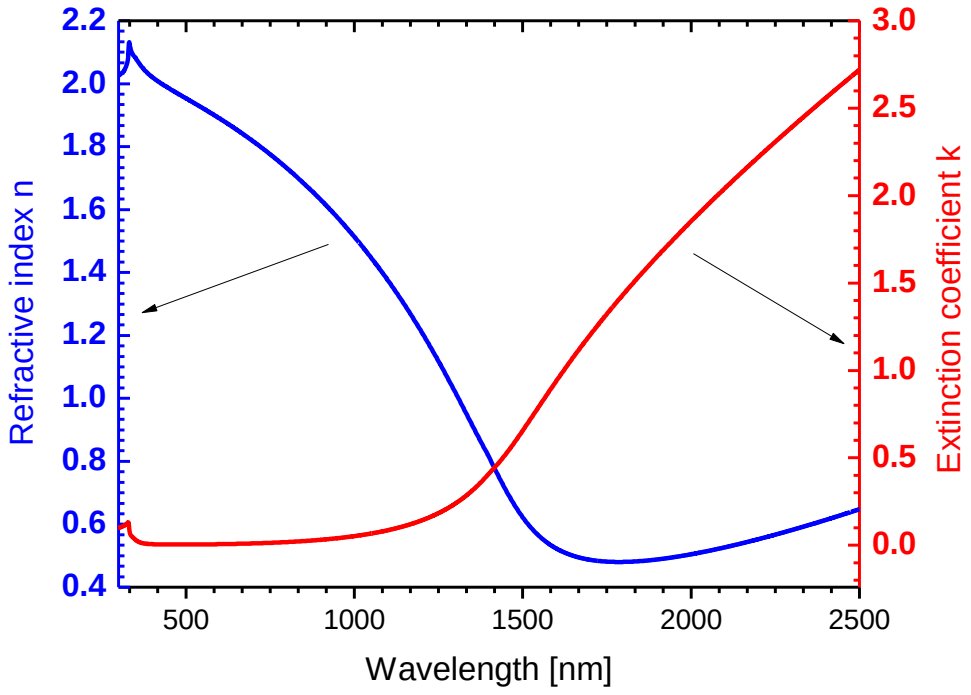

Figure 3.7: Optical constants n and k of AZO film derived from Drude-lorentz model fit

CHAPTER FOUR

COMPUTER SIMILATION OF RADIATIVE PROPERTIES OF AZO THIN FILMS

4.1 Introduction

In this chapter a computer simulation is carried out to calculate the radiative properties of Al doped ZnO (AZO) thin films nanostructure. The thermal emittance and solar absorptance is predicted indirectly from optical reflectance and transmittance of AZO films by invoking Kirchhoff's law as described in chapter two. A Special attention has been paid to the parameters that influence the spectral properties of the AZO films including film thickness, doping and carriers mobility. In the simulation the carriers mobility and the doping effect are taken independently but in real materials these two parameters are correlated.

4.2 Description of simulation method

The radiative properties of AZO films are calculated using the indirect approach based on Kirchhoff's law. The specific layered structure under consideration is depicted by figure 4-1.

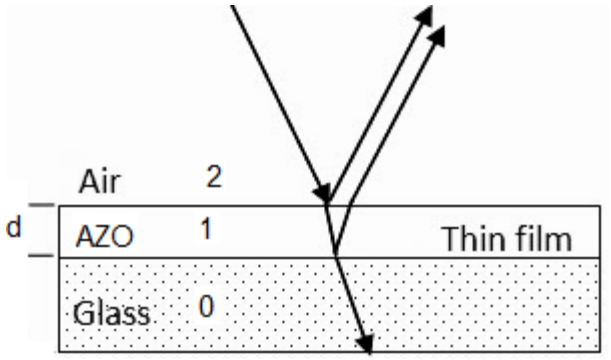

Figure 4.1: Schematic representation of the layered structure considered in the simulation.

AZO film, referred as medium 1, with a thickness d and described by a frequency-dependent dielectric function $\epsilon(\omega) = \epsilon'(\omega) + i\epsilon''(\omega)$ is coated on a glass substrate denoted as medium 0. The layered medium is considered perfectly smooth with sharp parallel interfaces and the AZO film is assumed homogeneous, isotropic and non-magnetic.

From Kirchhoff's law as described in chapter two, the spectral directional emissivity given by equation (2-13) can rewritten in terms of optical properties as

$$\varepsilon'(\lambda,\theta) = \frac{1}{2}\sum_{p=TE,TM}(1 - R^p - T^p) \qquad (4.1)$$

Where T and R are the optical transmittance and reflectance respectively in polarization state p (e.g. transvers electric TE and transvers magnetic TM) and λ and θ are the radiation wavelength and the incidence angle respectively. For bodies in local thermodynamic equilibrium according to Kirchhoff's law the spectral, directional emissivity is equal to the spectral, directional absorptivity α_λ (Modest et al, 2014).

Since the variation of emissivity with the azimuthal angle is usually negligible for an isotropic surface (Modest et al, 2014) equation (2-14) for the spectral hemispherical emissivity can be simplified as

$$\varepsilon(\lambda) = 2\int_{\theta=0}^{\frac{\pi}{2}} \varepsilon'(\lambda,\theta)cos\theta sin\theta d\theta \qquad (4.2)$$

For a diffuse surface the emissivity $\varepsilon'(\lambda)$ does not depend on direction.

The total hemispherical emissivity is then given by equation (2-19)

$$\varepsilon(T) = \frac{1}{\sigma T^4}\int_{0.3}^{30} \varepsilon_\lambda(\lambda,\mathrm{T})E_{\mathrm{b}\lambda}(\lambda,\mathrm{T})\,d\lambda$$

Where the integration interval is set from 0.3um to 30um for the simulation

To evaluate the absorptivity, the average solar illuminance on the earth surface is chosen as the spectral weight in the simulation under the condition of AM1.5 G (air mass=1.5) solar radiation spectrum $\boldsymbol{I_{sol}}$ as depicted in figure 1-1 chapter 1. The solar absorptivity is then defined as (Zhou et al, 2012)

$$\alpha_{sol} = \frac{\int_{0.3um}^{4um}\alpha(\lambda)I_{sol}d\lambda}{\int_{0.3um}^{4um}I_{sol}d\lambda} \qquad (4.3)$$

Where, the integrating interval is taken at a sufficient range to include the whole solar spectrum. By Kirchhoff's law $\alpha(\lambda)$ is regarded as $\varepsilon(\lambda)$.

To evaluate the performance of solar spectral selectivity of the AZO films a figure of merit is defined as (Nicholas et al, 2009)

$$F = \alpha_{sol}(1-\varepsilon(T)) \qquad (4.4)$$

And the optical efficiency of solar concentrator is defined as (Hall et al, 2012)

$$\eta = \alpha_{sol} - \frac{\int_{0.3um}^{30um}\varepsilon(\lambda)E_{\lambda b}d\lambda}{C\int_{0.3um}^{4um}I_{sol}d\lambda} \qquad (4.5)$$

Where C is the solar concentration ratio and $E_{\lambda b}$ is the spectral emissive power of a blackbody.

For the simulations a MATLAB program is developed (see figure 4.1) to calculate numerically the reflectance and transmittance of the AZO films by using transfer matrix method (Born et al, 1999). The dielectric function used in the simulation is given by equation 3.1 and the effect of plasma frequency wp, damping factor yo related to carrier mobility and the thickness of AZO films are on the performance of solar selectivity are investigated.

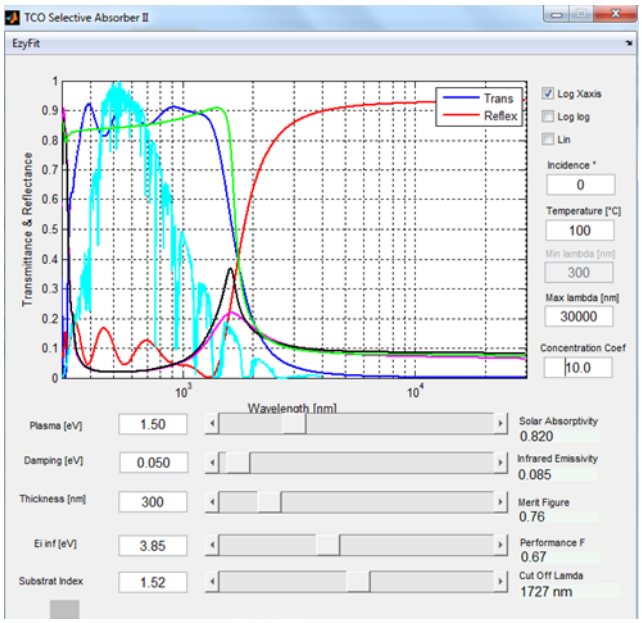

Figure 4.2: MATLAB© graphical interface developed for the simulation

4.3 Results and discussion

4.3.1 Effect of plasma frequency ω_p

The plasma frequency ω_p in AZO films depends on the extent of Al doping concentration. This frequency shifts towards higher energy when the concentration of Al is increased. This parameter is very crucial for application of AZO film as spectrally selective window in conjunction with a black body film absorber, because it controls the cut off wavelength λ_{cutoff} that defines the transition from semiconductor (insulating) state, where the transmittance is high, to metal state where the reflectance is high. For an ideal spectrally selective window the optical reflectance is close to 100% above λ_{cutoff} and 0% below λ_{cutoff} while it is the reverse for the optical transmittance. The simulated optical reflectance and transmittance at wavelengths ranging from 0.3 to 20 um are shown in Figure 4.3 for different values of plasma

frequency. In the simulation the film thickness and damping factor γ_0 are fixed to 300 nm and 0.1 eV respectively. The normalized AM15 solar spectrum I_{sol} and the normalized emissive power ***Eb*** for a blackbody at 300 °C are also included in the figure 4.3 where ***Eb*** peaks at wavelength of 5055 nm. At the plasma frequency of 0.5 eV (fig.4.3 a) the reflectance in the infrared spectrum is low and the cut-off wavelength located at about 3800 nm is crossing the black body emissive power spectrum which leads to a substantial radiative loss. In the VIS-NIR spectrum range the optical transmittance is high and averages to about 90% which allows a significant amount of solar intensity to be absorbed by the black body at the full solar spectrum. However this high absorbance is negated by high radiative loss of heat in the infrared range and therefor the AZO film is not spectrally selective.

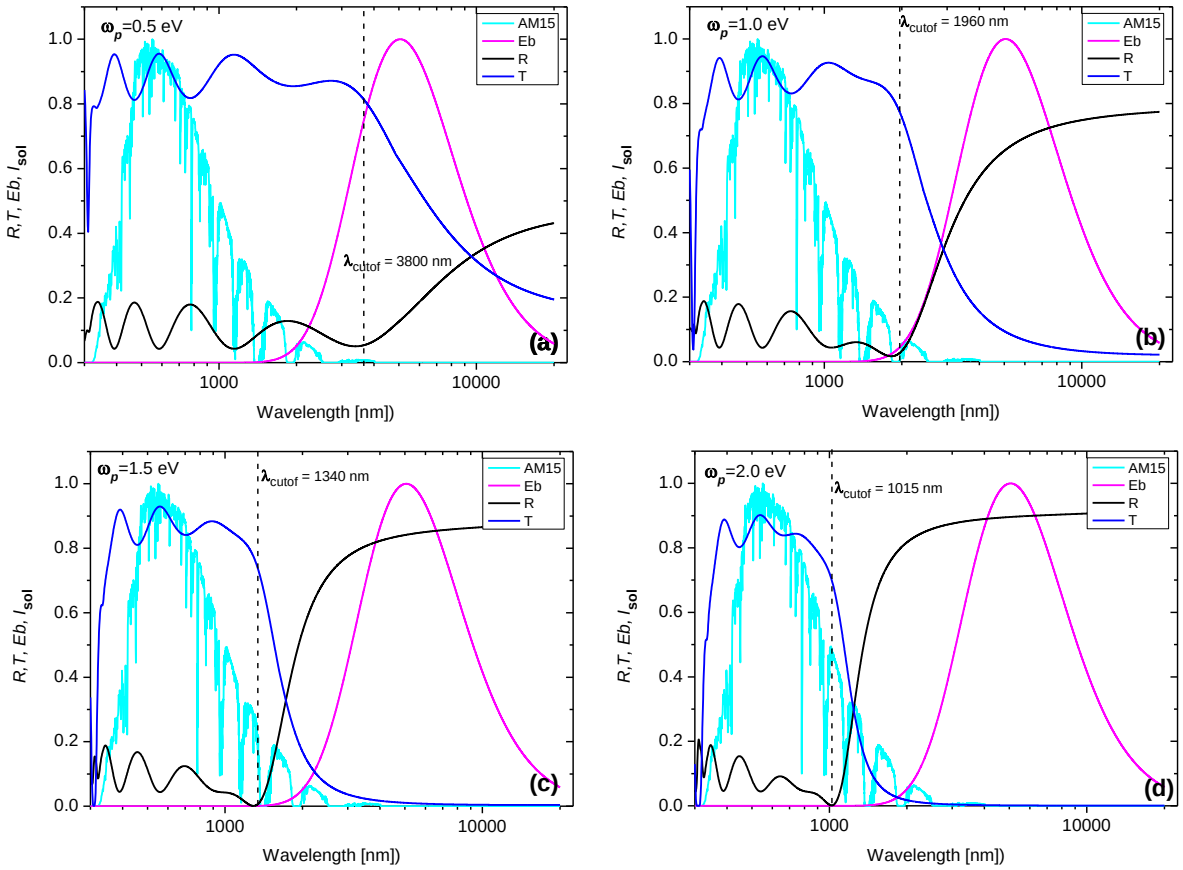

Figure 4.3: Simulated optical reflectance R and transmittance T of AZO films at different plasma frequencies (Al doping concentrations) and normalized AM15 solar spectrum I_{sol} and emissive power *Eb* for black body at 300 °C.

As the plasma frequency ω_p increases (fig 4.3 b,c,d) there is a clear shift of λ_{cutoff} to lower wavelength (higher energy) without crossing the black body emissive power spectrum which means the AZO film is spectrally selective for the black body at 300 °C. The optical reflectance is high and improves with the increase in plasma frequency yet the optical

transmission band is narrowing and the transmittance slightly decreases but remains still high. This band narrowing would affect the solar absorbance in a way that the solar spectrum is cropped at higher wavelengths and this will not contribute to the absorbance. For example in the case of ω_p = 2 eV (fig 4.3 d), about only 80% of the total integrated solar spectrum is available for absorbance, the remaining 20% gets reflected and absorbed by the AZO film.

As shown in the table 4.1 both the total hemispherical emissivity (eq. 2-19) and the absorptivity (eq. 4-3) decrease with an increase in ω_p**.** For a good spectrally selective thin film a lower emissivity and higher absorptivity are sought, consequently the plasma frequency has contradictious effect on the requirement for emissivity and absorptivity. As depicted by figure 4.4, the figure of merit as function of plasma frequency shows a bell shaped curve which peaks at wp =1.5 eV therefore the optimum plasma frequency for AZO thin films lies around a value of 1.5 eV where the figure of merit is higher (F= 0.68).

Table 4.1: Simulated effect of plasma frequency on total hemispherical emissivity and solar absorptivity in AZO films with a thickness of 300 nm and γ =0.1eV

ω_p [eV]	0.5	1	1.5	2
Total emissivity	0.33	0.24	0.15	0.11
Solar Absorptivity	0.88	0.87	0.80	0.69

4.3.2 Effect of damping factor (carrier mobility μ)

The damping factor γ (see eq. 3.1) is inversely proportional to carrier mobility μ in a material and is affected by the lattice vibration, impurity doping, defects, grain boundaries and electron-electron scattering (Hummel, 2001). The optical reflectance of metallic thin film depends on the carrier mobility (through relaxation time τ) as is given by equation 2-38. The simulated optical reflectance and transmittance at wavelengths ranging from 0.3 to 20 um are shown in Figure 4.5 for different values of damping factor. In the simulation the film thickness and the plasma frequency ω_p are fixed to 300 nm and 1.5 eV respectively.

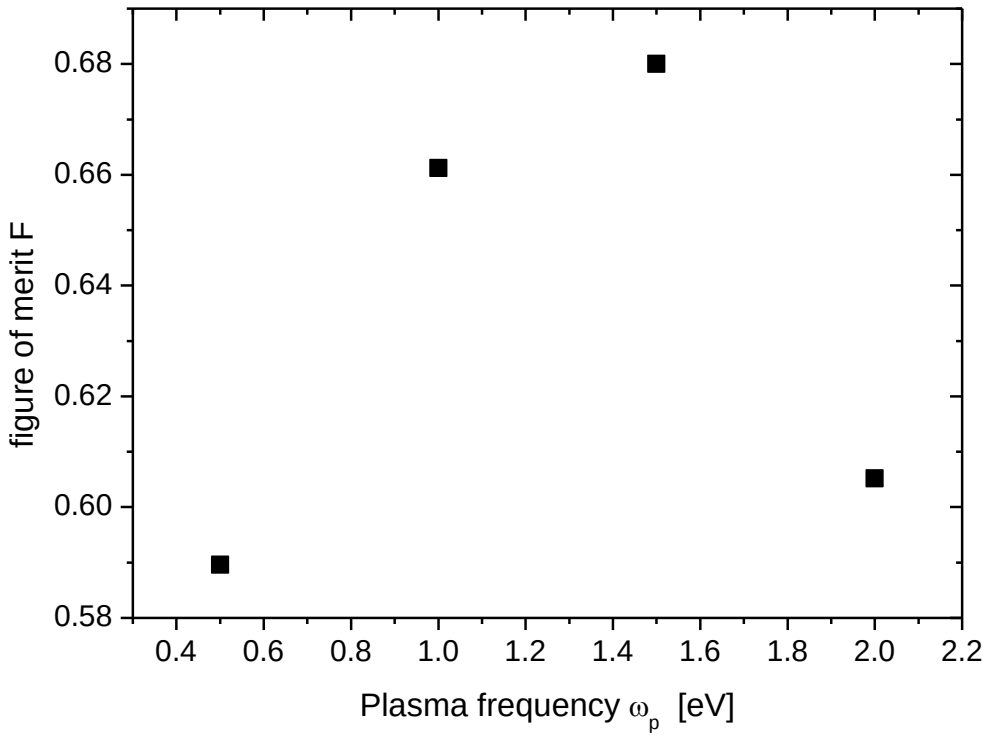

Figure 4.4: Figure of merit F versus plasma frequency

The cut off wavelength remains constant regardless of the variation of the damping factor. As the damping factor increases the transition of optical reflectance from low to high at λ_{cutoff} becomes more sluggish and the average reflectance in the infrared range decreases. At γ =0.05 eV (fig 4.5 a) the infrared reflectance levels at more than 90% while at γ=0.3 eV (fig 4.5 d) the level of reflectance is only 70%. Basically the average optical transmittance is high (about 85%) in the VIS-NIR range and remains unchanged regardless of the values of γ. However the onset of transmittance fall shifts towards lower wavelengths and consequently the optical transmission band gets narrower. The decline in the infrared reflectance and the reduction of the transmission band as γ rises, affect the radiative properties of AZO films as shown in table 4.2 and the merit figure as depicted by figure 4.6. The total hemispherical emissivity rises with damping factor while the solar absorptivity decreases. This leads to monotonous drops in the merit figure. The merit figure is substantially improved when γ is low (0.75 for γ =0.05 eV). Interestingly the highest merit figure of 0.85 is obtained for γ = 0 eV corresponding to infinite carrier mobility! Of course this case is unrealistic because the mobility in real materials is finite. Beside the impurity doping, the carrier mobility of AZO films depends heavily on the synthesis methods; and ranges from 10 to 50 $cm^2/V.s$ at room temperature (Irene, 2005) corresponding to a span of γ from 0.265 to 0.053 eV. This leads to a merit figure

ranging from 0.52 to 0.75 at room temperature for a film thickness of 300 nm and plasma frequency of 1.5 eV.

Table 4.2: Simulated effect of damping factor on total hemispherical emissivity and solar absorptivity in AZO films with a thickness of 300 nm and ω_p = 1.5 eV

γ [eV]	0.05	0.1	0.15	0.2	0.25	0.30	0.35
Total emissivity	0.09	0.15	0.21	0.26	0.29	0.32	0.34
Solar Absorptivity	0.82	0.80	0.77	0.75	0.73	0.72	0.70

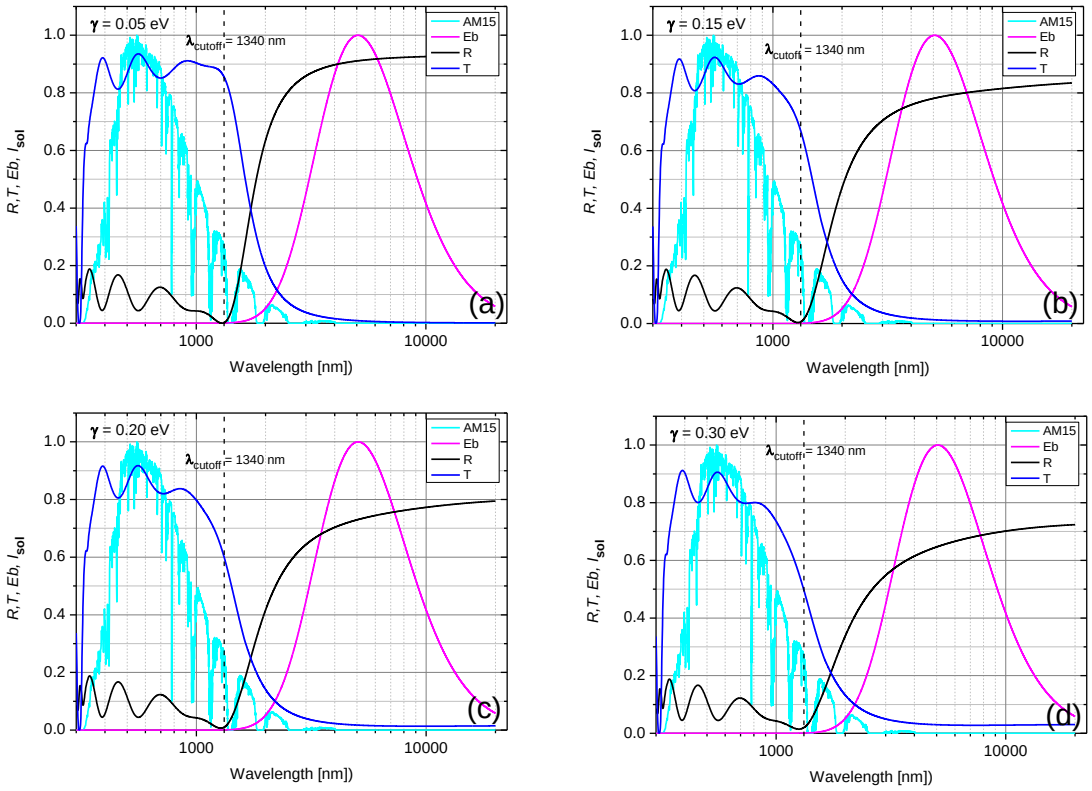

Figure 4.5: Simulated optical reflectance R and transmittance T of AZO films at different damping factors γ and normalized AM15 solar spectrum I_{sol} and emissive power Eb for black body at 300 °C.

Therefore, to obtain a higher merit figure, the carrier mobility in AZO films needs to be improved and one should notice that both carrier mobility and plasma frequency are dependent on the ionised impurity concentration.

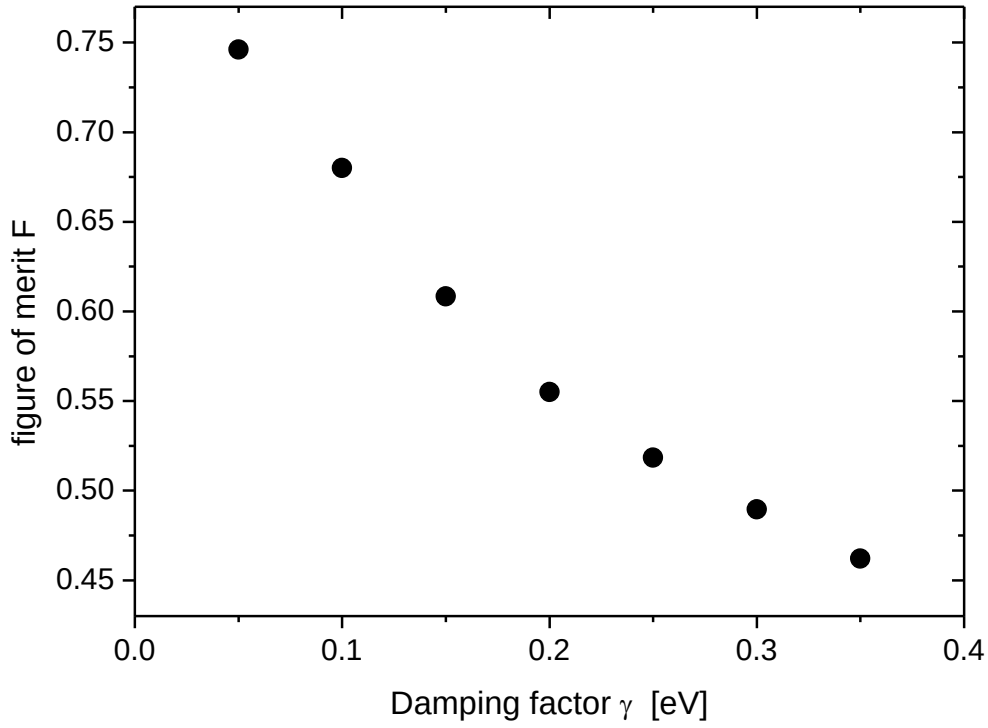

Figure 4.6: Figure of merit F versus damping factor

4.3.3 Effect of film thickness

As the thickness of a homogeneous thin film increases, light absorption increases also according to the Beer-Lamber-Law (Born et al, 1999). This will be reflected by a decrease in optical transmittance, however as far as the thickness of the film is higher than the skin depth (see chapter 2) the reflectance does not change with thickness (Hummel, 2001). The effect of the film thickness on the radiative properties of AZO films are summarized in table 4.3. The solar absorptivity decreases monotonously with the thickness increase, while the total hemispherical emissivity settles to 0.15 at thickness equal or higher than 300 nm. The variability in emissivity with thicknesses lower than 300 nm is probably due the skin depth which is a function of wavelength. As shown in figure 4.7 the merit figure F reaches a maximum of 0.69 at 200nm and then drops with the thickness increase. This is mostly due to the rise in solar absorptivity with the film thickness.

Table 4.3: Simulated effect of film thickness on total hemispherical emissivity and solar absorptivity in AZO films with γ = 0.1 eV and ω_p = 1.5 eV

Thickness nm	100	200	300	400	500	700	1000
Total emissivity	0.26	0.180	0.154	0.153	0.152	0.152	0.152
Solar Absorptivity	0.86	0.84	0.80	0.77	0.74	0.70	0.66

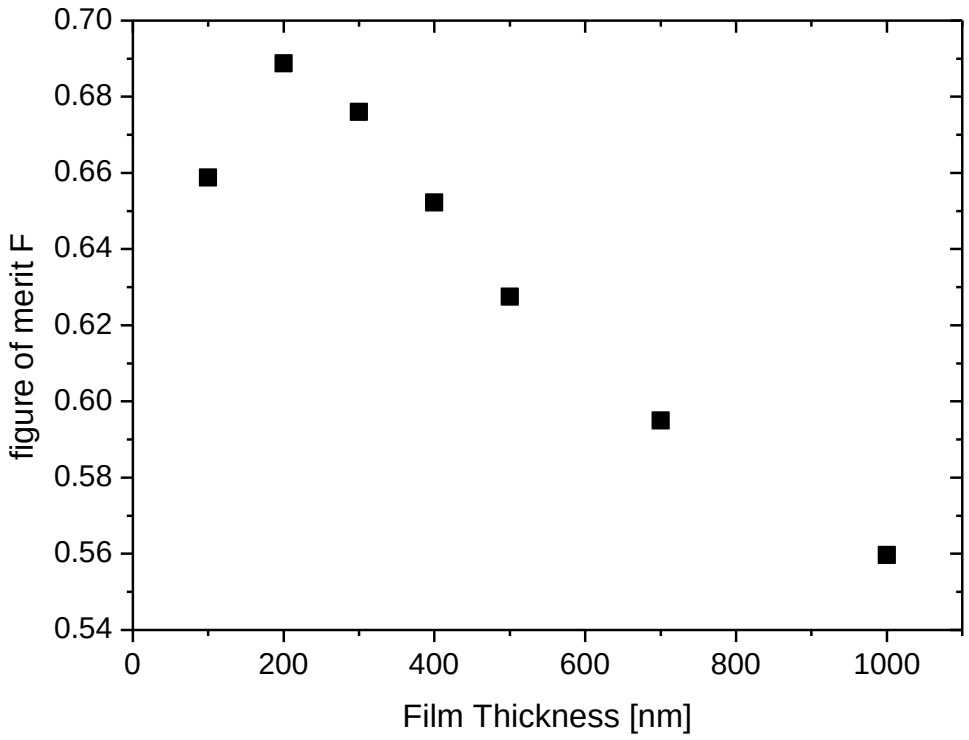

Figure 4.7: Figure of merit F versus AZO film thickness

4.3.4 Optimal parameters

From this numerical study we conclude that the best parameter values for obtaining higher figure of merit are ω_p =1.5 eV, γ = 0.05 eV and thickness of 200 nm. For these values, a merit figure of 0.78 is obtained with a total hemispherical emissivity of 0.10 and a solar absorptivity of 0.86. A comparison of data from figures 4.4, 4.6 and 4.7 shows that the damping factor γ has the most significant influence on the merit figure.

Using these optimal parameters a numerical evaluation of the optical performance η as a function of the solar concentration ratio C (eq. 4.5), is performed and plotted in figure 4.8. The performance η increases steeply with C lower than 30 and finally reaches a plateau of η =0.84 under C higher than 40.

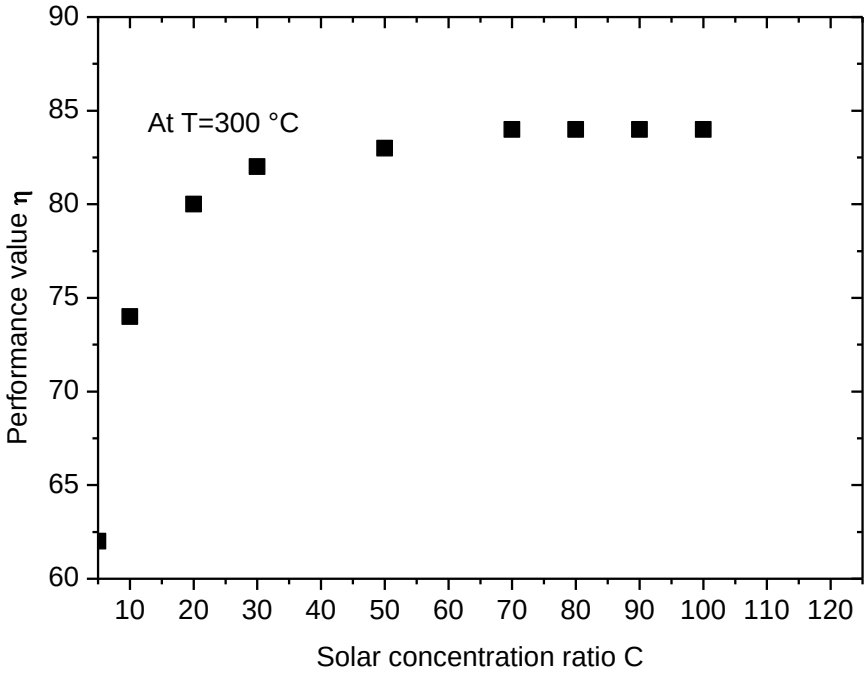

Figure 4.8: Calculated performance value η of AZO film as a function of solar concentration ratio C at 300 °C.

4.3.5 The total, directional emissivity

AZO films behave simultaneously as semiconductor (nonmetal) and metal therefore to perform a comparison of their radiative properties with the published data on nonmetal and metals. a numerical evaluation of the total directional emissivity given by equation 4-6 is performed on experimental AZO film described in chapter 3.

$$\varepsilon_s(T,\theta) = \frac{1}{\sigma T^4}\int_{0.3}^{\infty} \varepsilon'_\lambda(\lambda,\theta) E_{b\lambda}(\lambda,T)\, d\lambda \qquad (4.6)$$

For AZO film in semiconductor state the integration interval in eq.4.6 is set from 0.3um to λ_{cutoff} where the film is transparent and for AZO as metal the integration interval is chosen fromλ_{cutoff} to 30 um where the film is opaque. The calculated total directional emissivity for semiconductor and metal AZO film are depicted in polar form by in Figure. 4.9. For semiconductor state (fig 4.9 a) the directional emissivity varies little over a large range of incidence angles but decreases rapidly at grazing angles until a value of zero is reached at θ = π/2. Similar trends hold for metal state (fig. 4.9 b) except that, at grazing angles, the emissivity first increases sharply before dropping back to zero. Note that emissivity levels are considerably higher for nonmetals. These angular behaviors of the total directional emissivity

in the experimental AZO film is similar to the published directional emissivity experimentally determined for metals and nonmetals (Modest, 2014) as shown in figure 4.10

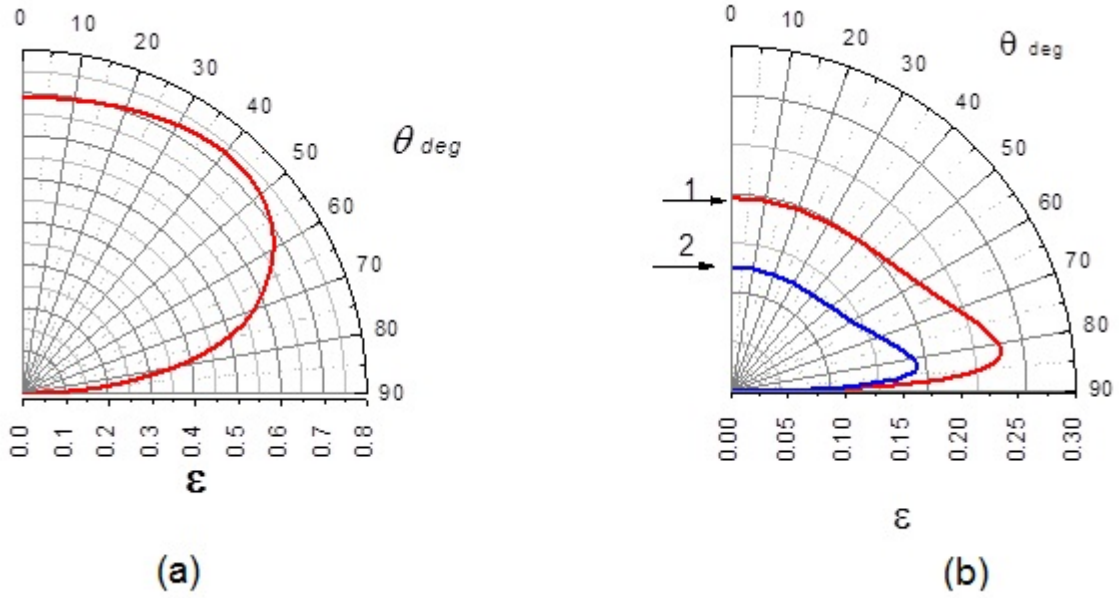

Figure 4.9: Calculated total directional emissivity as function of incidence angle θ (a) for experimental AZO film as nonmetal (semiconductor) (b) for experimental AZO film in metal state, curve 1 and optimized AZO film curve 2

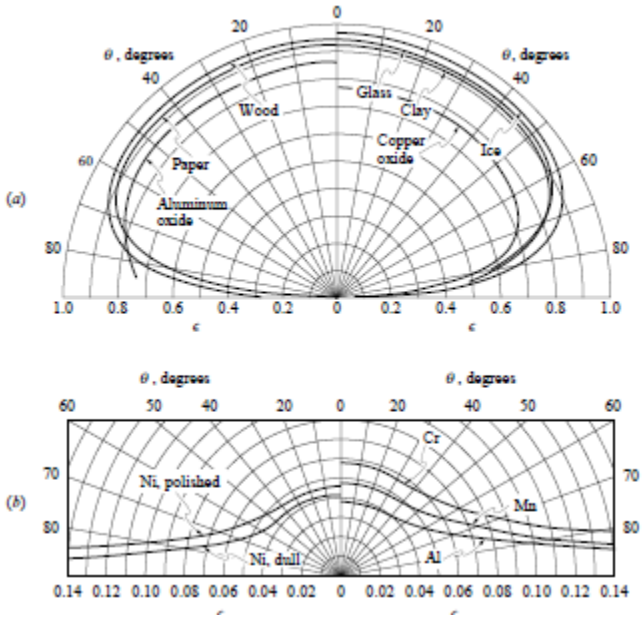

Figure 4.10: Directional variation of surface emissivity (a) for several nonmetals and (b) for several metals (Modest, 2014)

CHAPTER FIVE

CONCLUSIONS

Aluminum doped Zinc Oxide thin films are successfully deposited on soda lime glass substrates using RF magnetron sputtering. Through the investigation of the sputtering parameters the following conclusions are obtained.

- Regardless of the substrate temperature and the working gas pressure, All the AZO films exhibit a pronounced <00.l > fiber texture with the majority of the crystallites oriented along their crystallographic c-axis
- The higher crystalline quality and higher optical transmittance of the films deposited at 300°C is almost independent of the working pressure.
- The texture, crystalline quality and optical transmittance of the films deposited at RT show a strong dependence on the working gas pressure and they improve substantially with a decrease in Argon gas pressure.
- Independently of the substrate temperature the AZO films develop a compressive stress at lower working Ar gas pressure.
- The RT and the lower working gas pressure conditions for which a fair quality of the AZO films is obtained might be a promising route for the deposition of AZO films on flexible substrate.

Through the computer simulation, the thermal emittance and solar absorptance are predicted indirectly from optical reflectance and transmittance of AZO films by applying Kirchhoff's law and the following conclusions are drawn:

- Achieving higher solar absorptivity through AZO window and lower emissivity will depend strongly on higher carrier's mobility in AZO film.
- The emissivity levels to lower value when the films gets thick and increases when the film gets thinner. This is related the optical skin depth which varies with the wavelength. The optimal film thickness that gives higher spectral performance ranges from 200 nm to 300 nm.
- Increasing the carrier's concentration (by Al doping) will improve the sharpness of the optical reflectance at the cut off wavelength and hence the emissivity decreases rapidly. However the spectral performance does not necessarily improve because the solar absorptivity trough the AZO window decreases too.

Future work

In the simulation the mobility and doping are considered independently to simplify the calculation and get a general insight on their influence on the radiative properties of AZO film. However in real materials these two parameters are correlated and in future work this correlation will be taken in account to get a detailed insight of their effect on the spectral properties of TCO films.

References

(EIA), E. I. A. (2005). Annual Energy Review 2005.

Atkins, P., & Paula, J. de. (2010). Physical Chemistry (9th ed.). New York: W. H. Freeman and Company.

Bakos, G. C., Adamopoulos, D., Soursos, M., & Tsagas, N. F. (1999). Design and construction of a line-focus parabolic trough solar concentrator for electricity generation. In Proceedings of ISES solar world congress, Jerusalem.

Barlev, D., Vidu, R., & Stroeve, P. (2011). Innovation in concentrated solar power. Solar Energy Materials and Solar Cells, 95(10), 2703–2725. https://doi.org/10.1016/j.solmat.2011.05.020

Bergman, T. L., Lavine, A. S., Incropera, F. P., & DeWitt, D. P. (2011). Fundamentals of Heat and Mass Transfer. (L. Ratts & R. Marchione, Eds.) (7th ed.). New Jersey: John Wiley & Sons, Inc.

Bird, R. B., Stewart, W. E., & Lightfoot, E. N. (2002). Transport Phenomena (2nd ed.). New Jersey: John Wiley & Sons, Inc.

Born, M., Wolf, E. (1999). Principales of Optics. (7th ed). Cambridge: Cambridge Press University.

Brewster, M. Q. (1992). Thermal Radiative Transfer and Properties (1st ed.). New Jersey: John Wiley & Sons, Inc.

Brown, T. L., LEMay, H. E., Bursten, B. E., Murphy, C. J., & Woodward, P. M. (2012). Chemistry: the central science (12th ed.). New Jersey: Pearson Prentice Hall.

Cengel, Y. A. (2006). Heat and Mass Transfer: A Practical Approach (3rd ed.). New York: McGraw-Hill.

Cullity B.D.,. Stock S.R. (2014). Elements of X-Ray Diffraction. 3th ed. Essex: Pearson.

Duffie, J. A., & Beckman, W. A. (2013). Solar Engineering of Thermal Processes (4th ed.). New Jersey: John Wiley & Sons, Inc.

Edwards, P. P., Porch, A., Jones, M. O., Morgan, D. V., & Perks, R. M. (2004). Basic materials physics of transparent conducting oxides †. Dalton Trans., 2995–3002.

Foster, R., Cota, A., & Group, F. (2010). SOLAR and the Environment. Solar Energy.
Geankoplis, C. J. (1993). Transport Processes and Unit Operations. Prentice-Hall International (3rd ed.). New Jersey: Prentice-Hall International, Inc. Retrieved from http://books.google.com/books?id=i9-TQgAACAAJ&pgis=1

Giancoli, D. C. (2005). Physics: principles with appications (6th ed.). New Jersey: Pearson Prentice Hall.

Ginley, D. S., Bright, C., & Editors, G. (2000). Transparent Conducting Oxides. MRS Bulletin, (August), 15–18.

Gray, M. H., Tirawat, R., Kessinger, K. a., & Ndione, P. F. (2015). High Temperature Performance of High-efficiency, Multi-layer Solar Selective Coatings for Tower Applications. Energy Procedia, 69, 398–404. https://doi.org/10.1016/j.egypro.2015.03.046

Hall, A.C.; Ambrosini, A.; Ho, C.K.; McCloskey, J.F.; van Every, K.; McCloskey, J.F.; Urrea, D.A.; Lambert, T.N.; Bencomo, M.; Mahoney, A.R.; et al. (2012). Solar Selective Coatings for Concentrating Solar Power Central Receivers. *Adv. Mater. Process*., 170, 28–32.

Halliday, D., Resnick, R., & Walker, J. (2011). Fundamentals of physics. (S. Johnson & A. Rentrop, Eds.) (9th ed.). New Jersey: John Wiley & Sons, Inc.

Hepbasli, A., & Kalinci, Y. (2009). A review of heat pump water heating systems. Renewable and Sustainable Energy Reviews, 13(6–7), 1211–1229. https://doi.org/10.1016/j.rser.2008.08.002

Hollands, K. G. T. (2004). Thermal Radiation Fundamentals. BHB.

Holman, J. P. (2010). Heat Transfer (10th ed.). New York: McGraw-Hill Higher Education.

Hottel, H. C., Noble, J. J., Sarofim, A. F., Silcox, G. D., Wankat, P. C., & Knaebel, K. S. (2008).

Heat and Mass Transfer. In J. G. Knudsen & H. C. Hottel (Eds.), Perry's Chemical Engineers' Handbook (8th ed., pp. 5-1-5–83). New York: The McGraw-Hill Companies, Inc.

Howell, J. R., Menguc, M. P., & Siegel, R. (2016). Thermal Radiation Heat Transfer (6th ed.). Boca Raton: CRC Press Taylor Francis Group.

Hummel, R. E. (2001) .Electronic properties of materials. (3rd Ed.): New York: Springer

Incropera, F. P., DeWitt, D. P., Bergman, T. L., & Lavine, A. S. (2007). Fundamentals of Heat and Mass Transfer. Water (Vol. 6th). https://doi.org/10.1016/j.applthermaleng.2011.03.022

International Energy Agency IEA. (2011). Solar Energy Perspectives. Solar Energy Perspectives. OECD Publishing. https://doi.org/10.1787/9789264124585-en

Irene, E. A. (2005). Electronic Materials Science. Hoboken: John Wiley & Sons, Inc

Jagadish, C., Pearton, S. (2006). Zinc Oxide-Bulk, Thin Films and Nanostructures. New York: Elsevier Science

Kalogirou, S. a. (2004). Solar thermal collectors and applications. Progress in Energy and Combustion Science, 30(3), 231–295. https://doi.org/10.1016/j.pecs.2004.02.001

Kalogirou, S. a. (2014). Solar Energy Engineering processes and systems. Solar Energy Engineering (second edi). Elsevier. https://doi.org/10.1016/B978-0-12-374501-9.00014-5

Kennedy, C. E. (2002). Review of Mid- to High-Temperature Solar Selective Absorber Materials. Thechnical Report NREL (Vol. CP02.2000). Golden, CO. https://doi.org/10.2172/15000706

Kennedy, C. E., & Price, H. (2005). Progress in Development of High-Temperature Solar-Selective Coating. In Solar Energy (Vol. 2005, pp. 749–755). ASME. https://doi.org/10.1115/ISEC2005-76039

Kotz, J. C., Treichel, P. M., & Townsend, J. R. (2012). Chemistry & Chemical Reactivity (8th ed.). Belmont: Brooks/Cole Cengage Learning.

Kreith, F., & Kreider, J. F. (1978). Principles of solar engineering. Book.

Kreith, F., Manglik, R. M., & Bohn, M. S. (2011). Principles of Heat Transfer (7th ed.). Belmont: Brooks/Cole Cengage Learning.

Kudish, A. I., Santamaura, P., & Beaufort, P. (1985). Direct measurement and analysis of thermosiphon flow. Solar Energy, 35(2), 167–173.https://doi.org/10.1016/0038-092X(85)90006-4

Kuehn, T. H., Ramsey, J. W., & Threlkeld, J. L. (1998). Thermal Environmental Engineering (3rd ed.). New Jersey: Pearson Prentice Hall.

Levine, I. N. (2002). Physical chemistry (6th ed.). New York: McGraw-Hill Higher Education.

Lewis, B. G., & Paine, D. C. (2000a). A pplications and Processing of Transparent. MRS Bulletin, (August), 22–27.

Lewis, B. G., & Paine, D. C. (2000b). Applications and Processing of Transparent Conducting Oxides. MRS Bulletin, 25(8), 22–27. https://doi.org/10.1557/mrs2000.147

Mattox, D. M. (2010). The Low Pressure Plasma Processing Environment. In Handbook of Physical Vapor Deposition (PVD) Processing (pp. 157–193). Elsevier. https://doi.org/10.1016/B978-0-8155-2037-5.00005-8

Matzler, C. (2006). Thermal Microwave Radiation: Applications for Remote Sensing (Iee Electromagnetic Waves). The Institution of Engineering and Technology.

Modest, M. (2014). Radiative Heat Transfer (3rd ed.). Acedemic Press.

Nellis, G., & Klein, S. (2009). Heat Transfer. New Jersey: Cambridge University Press.

Nicholas P. Sergeant, Olivier Pincon, Mukul Agrawal, and Peter Peumans. (2009). Design of wide-angle solar-selective absorbers using aperiodic metal-dielectric stacks. *Optics Express*, 17(25), 22800

Norton, B. (2014). Harnessing Solar Heat, 18. https://doi.org/10.1007/978-94-007-7275-5

Nuru, Z. Y. (2013). Ph.D thesis University of the Western Cape Physics department Coatings for high temperature concentrated Solar power applications. University of Western Cape.

Nuru, Z. Y. (2014). Spectrally Selective AlXOY/Pt/AlXOY Soalr Absorber Coatings for High Temperature Solar-Thermal Applications. University of Western Cape.

Olsen, M. L., Warren, E. L., Parilla, P. a., Toberer, E. S., Kennedy, C. E., Snyder, G. J., … Ginley, D. S. (2014). A High-temperature, High-efficiency Solar Thermoelectric Generator Prototype. Energy Procedia, 49, 1460–1469. https://doi.org/10.1016/j.egypro.2014.03.155
Painuly, J. P. (2001). Barriers to renewable energy penetration ; a framework for analysis, 24, 73–89.

Patel, K., Patel, P., & Patel, J. (2012). Review of Solar Water Heating Systems. International Journal of Advanced Engineering Technology E, 3(4), 146–149.

Patent, U. S. (2014). Us 2010 / 0313875 A1, 2(12).

Petela, R. (2010). Engineering Thermodynamics of Thermal Radiation: for Solar Power Utilization (1st ed.). New York: McGraw-Hill Higher Education.

Raisul Islam, M., Sumathy, K., & Ullah Khan, S. (2013). Solar water heating systems and their market trends. Renewable and Sustainable Energy Reviews, 17, 1–25. https://doi.org/10.1016/j.rser.2012.09.011

Serway, R. A., & Jewett Jr., J. W. (2010). Physics for Scientists and Engineers with Modern Physics (8th ed.). Belmont: Brooks/Cole Cengage Learning.

Shimizu, M., Suzuki, M., Iguchi, F., & Yugami, H. (2014). High-temperature solar selective absorbers using transparent conductive oxide coated metal. Energy Procedia, 57, 418–426. https://doi.org/10.1016/j.egypro.2014.10.195

Shukla, R., Sumathy, K., Erickson, P., & Gong, J. (2013). Recent advances in the solar water heating systems: A review. Renewable and Sustainable Energy Reviews, 19, 173–190. https://doi.org/10.1016/j.rser.2012.10.048

Silbey, R. J., Alberty, R. A., & Bawendi, M. G. (2005). Physical Chemistry (4th ed.). New Jersey: John Wiley & Sons, Inc.

Smyth, M., Eames, P. C., & Norton, B. (2006). Integrated collector storage solar water heaters. Renewable and Sustainable Energy Reviews, 10(6), 503–538. https://doi.org/10.1016/j.rser.2004.11.001

Stadler, A. (2012). Transparent Conducting Oxides—An Up-To-Date Overview. Materials, (5), 661–683. https://doi.org/10.3390/ma5040661

Thekaekara, & P., M. (1970). The solar constant and the solar spectrum measured from a research aircraft.

Welty, J. R., Wicks, C. E., Wilson, R. E., & Rorrer, G. L. (2008). Fundamentals of Momentum, Heat, and Mass Transfer (5th ed.). New Jersey: John Wiley & Sons, Inc.

Windischmann, H. (1992). Intrinsic stress in sputter-deposited thin films. *Critical Reviews in Solid State and Materials Sciences,* 17(6), 547-596.

Yin, Y., & Collins, R. E. (1995). Optimization and analysis of solar selective surfaces with continuous and multilayer profiles. Journal of Applied Physics, 77(12), 6485. https://doi.org/10.1063/1.359124

Zhou WX, et al. Nano-Cr-film-based solar selective absorber with high photo-thermal conversion efficiency and good thermal stability. Opt Express 2012;20:28953.)

“Texas Energy Experts”. Internet: http://texasenergyexperts.com/solar-water-heater/
"PraguyNacorn". Internet: http://www.praguynakorn.com/product/3/sb-10 [Feb,2016].